


November 2015

Impact of Fabrication Parameters on the Internal Structure of Poly(3-hexylthiophene) Nanoparticles

Dana Desiree Algaier
University of Massachusetts - Amherst

Follow this and additional works at: https://scholarworks.umass.edu/dissertations_2

 Part of the [Materials Chemistry Commons](#), [Physical Chemistry Commons](#), and the [Polymer Chemistry Commons](#)

Recommended Citation

Algaier, Dana Desiree, "Impact of Fabrication Parameters on the Internal Structure of Poly(3-hexylthiophene) Nanoparticles" (2015). *Doctoral Dissertations*. 515.
https://scholarworks.umass.edu/dissertations_2/515

This Open Access Dissertation is brought to you for free and open access by the Dissertations and Theses at ScholarWorks@UMass Amherst. It has been accepted for inclusion in Doctoral Dissertations by an authorized administrator of ScholarWorks@UMass Amherst. For more information, please contact scholarworks@library.umass.edu.

**IMPACT OF FABRICATION CONDITIONS ON THE INTERNAL STRUCTURE
OF POLY(3-HEXYLTHIOPHENE) NANOPARTICLES**

A Dissertation Presented

by

Dana Desirée Algaier

Submitted to the Graduate School of the
University of Massachusetts Amherst in partial fulfillment
of the requirements for the degree of

DOCTOR OF PHILOSOPHY

September 2015

Department of Chemistry

© Copyright by Dana Desirée Algaier 2015

All Rights Reserved

**IMPACT OF FABRICATION CONDITIONS ON THE INTERNAL STRUCTURE
OF POLY(3-HEXYLTHIOPHENE) NANOPARTICLES**

A Dissertation Presented

by

DANA DESIRÉE ALGAIER

Approved as to style and content by:

Dhandapani Venkataraman, Chair

Paul M. Lahti, Member

Michael D. Barnes, Member

Anthony D. Dinsmore, Member

Craig T. Martin, Department Head
Chemistry

ABSTRACT

IMPACT OF FABRICATION PARAMETERS ON THE INTERNAL STRUCTURE OF POLY(3-HEXYLTHIOPHENE) NANOPARTICLES

SEPTEMBER 2015

DANA DESIRÉE ALGAIER, B.S., UNIVERSITY OF TENNESSEE KNOXVILLE

Ph.D., UNIVERSITY OF MASSACHUSETTS AMHERST

Directed by: Professor Dhandapani Venkataraman

Morphological control of organic functional materials is central to understanding and improving upon current technologies. The ability to create hierarchical assemblies with purposeful design from nano to meso scale has remained largely unattainable. This body of work aims to provide a foundation for creating nanoscale domains of poly (3-hexylthiophene) (P3HT) that can be used as building blocks to larger scale assemblies. We present a method for the fabrication of P3HT nanoparticles on the ability to vary the particle size and more importantly, the internal structure. We have identified the oil phase and surfactant as parameters able to influence the nature of P3HT aggregate within nanoparticles fabricated through the miniemulsion process.

TABLE OF CONTENTS

	Page
ABSTRACT	iv
LIST OF TABLES.....	vii
LIST OF FIGURES.....	viii
CHAPTER	
1. MODULAR APPROACH TO MORPHOLOGY	1
1.1 Introduction	1
1.2 Conjugated Nanoparticle Fabrication Methods	6
1.3 References	9
2. EFFECT OF FABRICATION PARAMETERS ON EXTERNAL CHARACTERISTICS OF P3HT NANOPARTICLES.....	14
2.1 Introduction	14
2.2 The Miniemulsion Method.....	15
2.3 Characterization Techniques	17
2.4 Fabrication Optimization	20
2.4.1 Sonication Time And Power	20
2.4.2 Surfactant Concentration	22
2.4.3 Polymer Concentration.....	24
2.4.4 Nature Of Polymer	25
2.5 Conclusion	26
2.6 References	28
3. EFFECT OF OIL PHASE ON THE INTERNAL STRUCTURE OF P3HT NANOPARTICLES.....	30
3.1 Introduction	30
3.2 Aggregate Information From Absorbance.....	30
3.3 Effect Of Solvent On Structure Of P3HT Thin Films	34
3.4 Effect of Solvent on P3HT Nanoparticles	36
3.5 Conclusion	41
3.6 References	42

4. EFFECT OF SURFACTANT ON THE INTERNAL STRUCTURE OF P3HT NANOPARTICLES.....	44
4.1 Introduction	44
4.2 Anionic Surfactant Chainlength	47
4.2.1 Temperature.....	49
4.2.2 Concentration.....	50
4.3 Cationic Surfactant Chainlength	52
4.3.1 Solubility of Surfactant in Oil Phase	54
4.4 Nonionic Surfactants.....	55
4.4.1 Triton X-45.....	56
4.4.2 CTAB-Triton Mixed Surfactant	59
4.4.3 Tomadol	60
4.5 Conclusion	61
4.6 References.....	63
5. FUTURE WORK	65
5.1 References.....	68
APPENDIX: EXPERIMENTAL SECTION	69
BIBLIOGRAPHY	74

LIST OF TABLES

Table	Page
3.1: Size, A0-0/A0-1 Intensity of P3HT Nanoparticles Synthesized from Different Solvent Composition	36
4.1: Log P values for linear alkanes and carboxylic acids of varying chain lengths (CRC handbook).....	47
4.2: Peak origin and ratio from UV-Vis, and size characterization of P3HT NPs made with Tomadol 91-8	61

LIST OF FIGURES

Figure	Page
1.1: Representation of the bulk heterojunction morphology meeting the requirements for interface and percolation of two component functional materials.....	1
1.2: Molecular structures of (A) poly (3-hexylthiophene) (P3HT) repeat unit, and (B) [6,6]-phenyl-C ₆₁ -butyric acid methyl ester (PCBM).	2
1.3: Comparison of the conventional method of fabricating films for OPVs through blending with limited control from molecular to nano –to- mesoscale to a modular nanoparticle approach allowing for each length scale to be designed and tuned independently. Reprinted from reference 45.	6
2.1: Cartoon of an enlarged emulsion droplet with phases and what is present.....	17
2.2: Diameter of P3HT NPs with increasing sonication time. Error bars represent the size distribution as half the Z-average peak width.....	21
2.3: Diameter of P3HT NPs with increasing sonication power. Error bars represent the distribution as half the Z-average peak width.	22
2.4: Diameter of P3HT NPs made with increasing surfactant concentration. Purple is Z-average, and green is the size distribution determined by the Z-average peak width. Error Bars are Standard deviation.....	23
2.5: Diameter of P3HT NPs made with increasing P3HT concentration. Purple is Z-average, and grey is the size distribution determined by the Z-average peak width. Error Bars are Standard deviation.	24
2.6: Diameter of polymer nanoparticles of varying molecular weight The polymers used in these experiments were synthesized by Dr. Feng Liu	25
2.7: Zeta potential of P3HT particles made of various molecular weights. The polymers used in these experiments were synthesized by Dr. Feng Liu	26

3.1: General energy diagram depicting the relative change in absorption due to transition dipole arrangement (black arrows) of dimeric identical chromophores. Recreated from discussions with Dr. Joelle Labastide and Professor Michael Barnes	31
3.2: (left) Molecular depiction of thiophene packing with arrows in the direction of interchain (H-aggregate) and intrachain (J-aggregate) coupling. (right) Recreated absorption spectra of pure H and J aggregates of P3HT with 0-0 and 0-1 transition peaks labeled.....	33
3.3: Absorption spectra of P3HT in chloroform (orange), spun cast thin film (purple) and nanoparticle dispersion (black filled) with peaks marked.....	35
3.4: (top) Normalized absorption spectra of P3HT nanoparticles made from chloroform, toluene, and 1:4 mixture of toluene to chloroform. (bottom) open-circle line and closed-circle line show the amorphous absorption and aggregate absorption respectively in each nanoparticle spectra. Vertical dashed line indicates the A_{0-2} peak position (520 nm) and separates the solvent-quality independent part of the absorption spectra from the region that is fairly affected by solvent. Reprinted from reference 13.....	38
3.5: UV-vis absorption spectra of P3HT in various solvents. The presence of a peak around 610 nm indicates the presence of P3HT aggregates. The sizes of the P3HT aggregates measured by dynamic light scattering of 0.5 wt % P3HT solution in different solvents are shown in the figure key. For clarity absorption spectra is shown between 560 and 660 nm. Reprinted from Reference 13.	39
3.6: Recreated from TRPL results on single nanoparticles from reference 13. The range of slow time component is plotted by fast time component from nanoparticles made from various solvents and lowering the evaporation temperature.	41
4.1: Molecular structures and absorbance of nanoparticles made with sodium dodecyl sulfate (SDS in black) and cetyltrimethylammonium bromide (CTAB in red)	44
4.2: Possible scenarios for surfactant to affect the internal structure of the nanoparticle.	45

4.3: Sodium sulfate surfactant head group with a series of linear hydrocarbon chains.	47
4.4: Comparison of percent aggregate and peak ratio* as determined by UV-vis absorbance, and size characteristics of P3HT nanoparticles made with sodium sulfate head group surfactants with varying length of hydrocarbon tail C8 (red), C12 (yellow), C14 (green) C18(purple). Error bars represent standard deviation	48
4.5: UV absorbance of C8, C12, C18 SDS surfactants with varying evaporation temperature.....	50
4.6: UV-Vis absorbance of P3HT nanoparticles made with 10 mM (black) and 1 mM (green) surfactant concentration of C8, C12, C18 Chainlengths.	51
4.7: P3HT nanoparticles made with CTAB type surfactants varying the hydrocarbon chain length C12 (green), C14 (purple) and C16 (red).	52
4.8: Particle size of nanoparticles made with CTAB type C12 chainlength surfactant.....	53
4.9: Absorbance Spectra of P3HT in CHCl ₃ with the addition of CTAB over time, t=0 min (red), t=5 min (blue), t=8 min (green).....	54
4.10: Critical packing parameter for amphiphiles, geometry defines what shape micelle to expect for self-assembly in water.....	55
4.11: Molecular structure of nonionic surfactant, Triton X-45	55
4.12: Absorbance spectra of P3HT NPs made with decreasing concentration of Triton X-45	56
4.13: SEM images of nanoparticles made with nonionic surfactant. P3HT particles made with Triton X-45 (left) and polystyrene particles made with Tomadol 25-7 (right). The pink boxes are the areas EDAX was done on.....	57
4.14: SEM image of possible NaCl crystals from dropcasting a dispersion of P3HT NPs, drying under air followed by a water rinse.....	58

4.15: Confocal Fluorescence Microscopy images of P3HT particles made with Triton X-45 (left) light illumination (right) fluorescent image	58
4.16: %Aggregate P3HT and A_{0-0}/A_{0-1} peak ratio from (x100) absorbance of P3HT NPs made with mixed surfactant of CTAB and Triton.....	59
4.17: SEM of P3HT “NPs” made with varying ratios of CTAB to Triton 50/50(left), 70/30 (middle and right).....	60
4.18: Molecular structure of Tomadol-91-8.....	60
4.19: SEM of P3HT NPs clogging syringe filter membranes.	61
5.1: HRTEM image of a 116 nm particle. Crystalline domains of about 5–10 nm have been highlighted. The insets display the crystalline arrangements of each crystal. From these images, it is evident that the internal crystalline domains are randomly oriented.....	65

CHAPTER 1

MODULAR APPROACH TO MORPHOLOGY

1.1 Introduction

Organic electronic materials continue to advance current technologies in applications such as light-emitting diodes (OLEDs)^{1,2}, photovoltaic cells (OPVs)^{3,4}, sensors⁵, thin film transistors⁶, thermoelectric materials⁷ and many more.⁸⁻¹⁰ A key aspect of organic electronic materials is that their electronic properties are governed by the organization of molecules in solid state¹¹⁻¹³. It is a challenge to control the molecular organization in the solid state and the challenge is amplified by the need for a hierarchy to the molecular organization. For example, in OPVs, the device performance is dictated by the active layer morphology¹⁴⁻¹⁷, which is not easily predicted or controlled. At the start of this project and still to date the most commonly used morphology is the bulk



Figure 1.1: Representation of the bulk heterojunction morphology meeting the requirements for interface and percolation of two component functional materials.

heterojunction (BHJ) (pictured in Figure 1.1). This is because BHJ provides nanoscale domains of a donor and acceptor material as well as continuous pathways for charges to be moved to the electrodes. OPVs' archetypal system, a semi-crystalline polymer, poly (3-hexylthiophene) (P3HT) and a fullerene based small molecule [6,6]-phenyl-C₆₁-butyric acid methyl ester (PCBM) (Figure 1.2) is known to reliably make BHJ type structures.^{18,19}

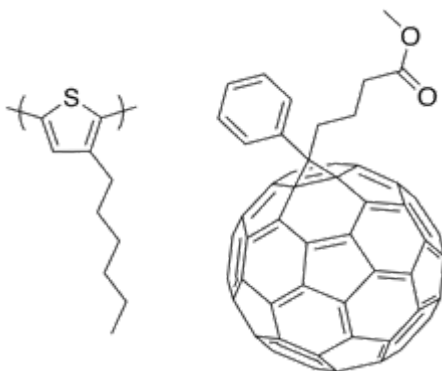


Figure 1.2 Molecular structures of (A) poly (3-hexylthiophene) (P3HT) repeat unit, and (B) [6,6]-phenyl-C₆₁-butyric acid methyl ester (PCBM).

Tuning the morphology of P3HT/PCBM has been the focus of numerous studies, which have flooded the literature with structure-function correlations between the molecular scale packing and its relation to efficiency.^{20–24} However, with the synthesis of new promising materials, i.e. low-bandgap polymers, non-fullerene based acceptors, the morphological lessons learned from P3HT-PCBM systems are not easily applied. Consequently, the challenge of morphological control on multiple length scales continues to be addressed on a narrow, case-by-case basis. Furthermore the very nature of P3HT — its molecular weight^{25–28}

and regioregularity^{28,29} —has a drastic impact on the molecular packing, thus the electronic coupling, making the game of morphological control even more challenging and crucial. Given the complexity of intermolecular mixing the field is in need of a general method to assemble nanoscale domains that can be extended to mesoscale assemblies independent of molecular properties.

Several bottom up strategies have been employed to conquer this major roadblock in organic functional materials, mainly relying on molecular scale non-covalent interactions programmed into the material by synthetic design.^{30–35} One of the pioneering approaches to exert control in the self-assembly of two molecules is to covalently link them as a block copolymer (BCP).³⁶ Inspiration from the well studied self-assembly of amphiphilic molecules led to the idea of using intramolecular induced phase separation in BCP systems. In addition, it has been shown that much like traditional amphiphilic molecules one can tune the interactions in such a way to produce predictable nanoscale domains with mesoscale order. The ability to change the overall bulk morphology arises from reaching an equilibrium state that minimizes the interfacial energy. The most diverse and predictable BCP phase diagram is restricted to immiscible blocks of coil-coil polymers that intrinsically have a large amount of conformational and rotational freedom along the main chain backbone.³⁷ Unfortunately, this beautifully predictable self-assembly falls apart for electronically functional materials, i.e., semi-crystalline conjugated polymers in part due to their inherently rigid structure. And the level of phase predictability becomes increasingly

complicated because of a myriad of non-covalent intermolecular interactions; H-bonding, π - π stacking, crystallization, electrostatics, hydrophilic and hydrophobic effects, sterics, and stiffness asymmetry.³⁴ Unconventional structures can be obtained when using conjugated polymer blocks however the method lacks grace, reducing the idea of molecular architecture to a mere guessing game.

We set out to establish a general strategy for morphological control of conjugated organic materials that provides predefined nanoscale domains while being able to extend the system to mesoscale morphologies.^{38,39} Much like the construction of a building we first fabricate building blocks of our design and level the morphological playing field by relying on predictable geometric self assembly instead of unpredictable molecular scale self-assembly interactions. (Figure 1.3)

The idea of using geometry to control structures descends from Linus Pauling who proposed in 1929 that the radius ratio ($R_{\text{cation}}/R_{\text{anion}}$) as a predictive tool for ordered structures of ionic crystals.⁴⁰ Extending the idea of geometrical packing to nanoscale spheres has been shown in spherical inorganic nanoparticles without the need for electrostatic interactions.⁴¹⁻⁴⁴ Although it may seem counterintuitive, a major driving for the ordering of spheres in to a lattice is an entropic gain, explained by greater free-volume entropy for each particle. Given nearly monodisperse nanoparticles (<10%), the structural diversity of ordered binary nanoparticle superlattices (BNSLs) is governed simply by the number ratio of particles and ratio of particle radii. We bring to bear the exciting

principles of geometry on the problem of morphology control in electronic devices.

We are interested in employing this same strategy in organic systems, by performing molecular assemblies into nanoscale domains and utilizing geometric packing to create mesoscale assemblies of our design. This modular approach to nanostructures of organic functional materials, specifically conjugated polymers, enables (1) the single step assembly of two or more spherical components into stable nanostructures; (2) independent fabrication of molecular assemblies in predetermined domain sizes dictated by NP size, (3) methodical adjustments of the nanoscale morphology via altering the particle shape and size: and (4) the power to logically design and produce multicomponent nanostructured materials. In order to design and create mesoscale assemblies of nanoscale domains we first need a method to fabricate nanoparticles.

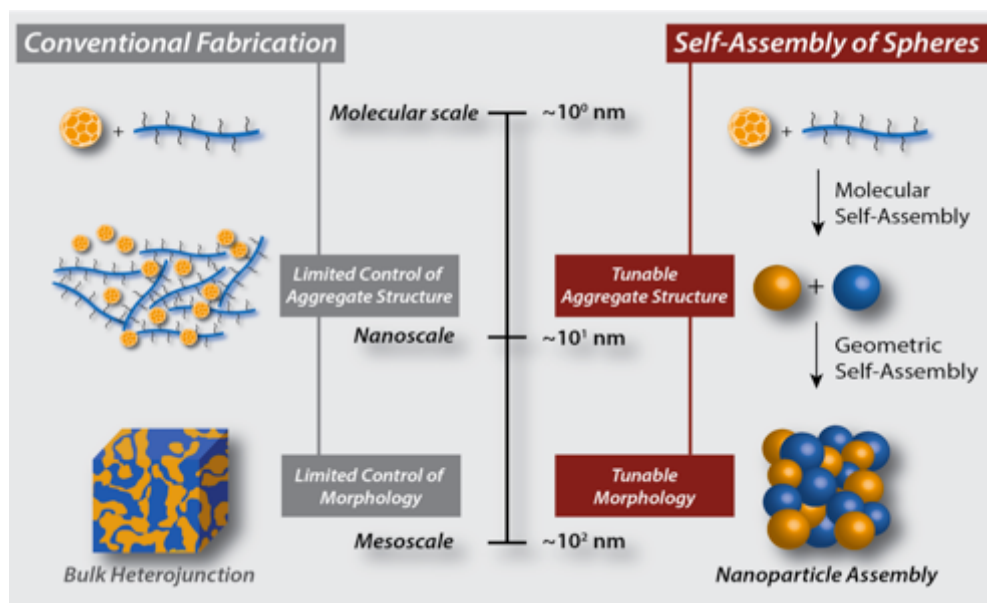


Figure 1.3: Comparison of the conventional method of fabricating films for OPVs through blending with limited control from molecular to nano –to-mesoscale to a modular nanoparticle approach allowing for each length scale to be designed and tuned independently. Reprinted from reference 45.

1.2 Conjugated Nanoparticle Fabrication Methods

There are many methods available to fabricate conjugated polymer nanoparticles.⁴⁶ Three main methods used for making nanoparticles of preformed polymers are reprecipitation⁴⁸, aerosol/nebulization⁴⁹, and miniemulsion.⁴⁷ Reprecipitation requires dissolving the preformed polymer in a water miscible solvent, injecting the solution into an aqueous solution and evaporating the solvent causing polymer chain collapse at the oil- water interface. Ultimately the particles obtained reflect the nature of the polymer in the oil phase and the miscibility of the oil in water.⁴⁶ Nebulization techniques have been shown to make nearly monodisperse polymer particles and the amount of polymer and flow rate

used controls the size.⁴⁷ This method, similar to reprecipitation, involves chain collapse, but the chain collapse occurs at the air-oil interface instead of the water-oil interface. In both methods, we are limited by scalability and a general way to tune particle properties made of any kind of conjugated polymer.⁴⁸⁻⁵¹

Miniemulsion utilizes a water-immiscible solvent and a surfactant to stabilize the emulsion. Miniemulsion affords solvent annealing within a droplet along with other parameters to tune, including in-situ synthesis. The nanoparticle (NP) size comes from what is contained in a stabilized droplet.^{52,53} Droplet stabilization is the minimization of interfacial tension between oil and water and is achieved by use of surfactants and/or colloidal particles. The droplet size distribution, in theory, can be monodisperse but there are competing forces afoot. Droplets with insufficient protection can coalesce to form larger droplets, and the diffusion of smaller droplets into larger droplets, Ostwald Ripening. This process lowers the total interfacial surface area and Laplace Pressure of the system. The surfactant coverage must be sufficient to lower the free energy and come to a steady-state to discourage the above-mentioned processes. Overall, miniemulsion affords the most on control over nanoparticle fabrication through solvent annealing of polymer in the stabilized droplet, a variety of tunable parameters, and the ability to scale up production.

The work presented in this thesis looks at the design and fabrication of our building blocks, conjugated polymer nanoparticles (CP NPs) with the overarching application of OPV. Given our fabrication method of choice, miniemulsion, we

need to know how this method can influence our nanoparticles. First, we want to know which parameters of the miniemulsion can be varied in order to control the external characteristics, size, size distribution and stability, of the nanoparticles. Once we have established an optimized method of making CPNPs our focus is turned inward. We are interested in how we can alter the molecular packing of P3HT with in a particle. Chapter 3 looks at the effect of the oil phase on internal structure. The results can also shed light on the miniemulsion process through comparison to the solvent dependence of P3HT morphology in thin films. In the remaining chapters we explore the influence of surfactant type on the internal structure of CPNPs. Although surfactant has the possibility of interacting in all phases of the miniemulsion, its role in the formation of nanoparticles and their resulting structures is unknown. Ideally, this body of work paves the way for straightforward design and fabrication of conjugated polymer nanoparticle domains enabling tunable morphology previously unobtainable in organic materials.

1.3 References

- (1) Jou, J.-H.; Kumar, S.; Agrawal, A.; Li, T.-H.; Sahoo, S. Approaches for fabricating high efficiency organic light emitting diodes. *J. Mater. Chem. C* **2015**, *3*, 2974–3002.
- (2) Reineke, S.; Lindner, F.; Schwartz, G.; Seidler, N.; Walzer, K.; Lüssem, B.; Leo, K. White organic light-emitting diodes with fluorescent tube efficiency. *Nature* **2009**, *459*, 234–238.
- (3) Søndergaard, R. R.; Hösel, M.; Krebs, F. C. Roll-to-Roll fabrication of large area functional organic materials. *J. Polym. Sci. Part B Polym. Phys.* **2013**, *51*, 16–34.
- (4) Jackson, N. E.; Savoie, B. M.; Marks, T. J.; Chen, L. X.; Ratner, M. A. The Next Breakthrough for Organic Photovoltaics? *J. Phys. Chem. Lett.* **2015**, *6*, 77–84.
- (5) Lee, J.; Balakrishnan, S.; Cho, J.; Jeon, S.; Kim, J. Detection of adulterated gasoline using colorimetric organic microfibers. *J. Mater. Chem.* **2011**, *21*, 2648.
- (6) Khim, D.; Baeg, K.-J.; Caironi, M.; Liu, C.; Xu, Y.; Kim, D.-Y.; Noh, Y.-Y. Control of Ambipolar and Unipolar Transport in Organic Transistors by Selective Inkjet-Printed Chemical Doping for High Performance Complementary Circuits. *Adv. Funct. Mater.* **2014**, *24*, 6252–6261.
- (7) Chen, Y.; Zhao, Y.; Liang, Z. Solution processed organic thermoelectrics: towards flexible thermoelectric modules. *Energy Environ. Sci.* **2015**, *8*, 401–422.
- (8) Mecerreyes, D. Polymeric ionic liquids: Broadening the properties and applications of polyelectrolytes. *Prog. Polym. Sci.* **2011**, *36*, 1629–1648.
- (9) Jochum, F. D.; Theato, P. Temperature- and light-responsive smart polymer materials. *Chem. Soc. Rev.* **2013**, *42*, 7468–7483.
- (10) Ikkala, O.; ten Brinke, G. Functional materials based on self-assembly of polymeric supramolecules. *Science* **2002**, *295*, 2407–2409.
- (11) Kim, J.; Swager, T. Control of conformational and interpolymer effects in conjugated polymers. *Nature* **2001**, *411*, 1030–1034.

- (12) Hong, Y.; Lam, J. W. Y.; Tang, B. Z. Aggregation-induced emission: phenomenon, mechanism and applications. *Chem. Commun.* **2009**, 4332.
- (13) Spano, F. C. Excitons in conjugated oligomer aggregates, films, and crystals. *Annu. Rev. Phys. Chem.* **2006**, *57*, 217–243.
- (14) Noriega, R.; Rivnay, J.; Vandewal, K.; Koch, F. P. V.; Stingelin, N.; Smith, P.; Toney, M. F.; Salleo, A. A general relationship between disorder, aggregation and charge transport in conjugated polymers. *Nat. Mater.* **2013**, *12*, 1038–1044.
- (15) Benanti, T. L.; Venkataraman, D. Organic solar cells: an overview focusing on active layer morphology. *Photosynth. Res.* **2006**, *87*, 73–81.
- (16) Nagarjuna, G.; Venkataraman, D. Strategies for controlling the active layer morphologies in OPVs. *J. Polym. Sci. Part B Polym. Phys.* **2012**, *50*, 1045–1056.
- (17) Huang, Y.; Kramer, E. J.; Heeger, A. J.; Bazan, G. C. Bulk heterojunction solar cells: morphology and performance relationships. *Chem. Rev.* **2014**, *114*, 7006–7043.
- (18) Dang, M. T.; Hirsch, L.; Wantz, G. P3HT:PCBM, Best Seller in Polymer Photovoltaic Research. *Adv. Mater.* **2011**, *23*, 3597–3602.
- (19) Dennler, G.; Scharber, M. C.; Brabec, C. J. Polymer-fullerene bulk-heterojunction solar cells. *Advanced Materials*, 2009, *21*, 1323–1338.
- (20) Zhokhavets, U.; Erb, T.; Gobsch, G.; Al-Ibrahim, M.; Ambacher, O. Relation between absorption and crystallinity of poly(3-hexylthiophene)/fullerene films for plastic solar cells. *Chem. Phys. Lett.* **2006**, *418*, 347–350.
- (21) Moulé, a. J.; Meerholz, K. Controlling Morphology in Polymer–Fullerene Mixtures. *Adv. Mater.* **2008**, *20*, 240–245.
- (22) Dang, M. T.; Hirsch, L.; Wantz, G.; Wuest, J. D. Controlling the Morphology and Performance of Bulk Heterojunctions in Solar Cells. Lessons Learned from the Benchmark Poly(3-hexylthiophene):[6,6]-Phenyl-C 61 -butyric Acid Methyl Ester System. *Chem. Rev.* **2013**, *113*, 3734–3765.
- (23) Servaites, J. D.; Ratner, M. a.; Marks, T. J. Organic solar cells: A new look at traditional models. *Energy Environ. Sci.* **2011**, *4*, 4410.

- (24) Yin, W.; Dadmun, M. A New Model for the Morphology of P3HT/PCBM Organic Photovoltaics from Small-Angle Neutron Scattering: Rivers and Streams. *ACS Nano* **2011**, *5*, 4756–4768.
- (25) Scharsich, C.; Lohwasser, R. H.; Sommer, M.; Asawapirom, U.; Scherf, U.; Thelakkat, M.; Neher, D.; Köhler, A. Control of aggregate formation in poly(3-hexylthiophene) by solvent, molecular weight, and synthetic method. *J. Polym. Sci. Part B Polym. Phys.* **2012**, *50*, 442–453.
- (26) Panzer, F.; Bäessler, H.; Lohwasser, R.; Thelakkat, M.; Köhler, A. The Impact of Polydispersity and Molecular Weight on the Order–Disorder Transition in Poly(3-hexylthiophene). *J. Phys. Chem. Lett.* **2014**, *5*, 2742–2747.
- (27) Paquin, F.; Yamagata, H.; Hestand, N. J.; Sakowicz, M.; Bérubé, N.; Côté, M.; Reynolds, L. X.; Haque, S. a.; Stingelin, N.; Spano, F. C.; et al. Two-dimensional spatial coherence of excitons in semicrystalline polymeric semiconductors: Effect of molecular weight. *Phys. Rev. B - Condens. Matter Mater. Phys.* **2013**, *88*, 155202.
- (28) Zhao, K.; Xue, L.; Liu, J.; Gao, X.; Wu, S.; Han, Y.; Geng, Y. A New Method to Improve Poly(3-hexyl thiophene) (P3HT) Crystalline Behavior: Decreasing Chains Entanglement to Promote Order-Disorder Transformation in Solution. *Langmuir* **2010**, *26*, 471–477.
- (29) Woo, C. H.; Thompson, B. C.; Kim, B. J.; Toney, M. F.; Fréchet, J. M. J. The influence of poly(3-hexylthiophene) regioregularity on fullerene-composite solar cell performance. *J. Am. Chem. Soc.* **2008**, *130*, 16324–16329.
- (30) Lecover, R.; Williams, N.; Markovic, N.; Reich, D. H.; Naiman, D. Q.; Katz, H. E. Next-generation polymer solar cell materials: Designed control of interfacial variables. *ACS Nano* **2012**, *6*, 2865–2870.
- (31) He, Z.; Wu, H.; Cao, Y. Recent advances in polymer solar cells: realization of high device performance by incorporating water/alcohol-soluble conjugated polymers as electrode buffer layer. *Adv. Mater.* **2014**, *26*, 1006–1024.
- (32) Evans, R. C. Harnessing self-assembly strategies for the rational design of conjugated polymer based materials. *J. Mater. Chem. C* **2013**, *1*, 4190.

- (33) Schacher, F. H.; Rugar, P. A.; Manners, I. Functional block copolymers: nanostructured materials with emerging applications. *Angew. Chemie Int. Ed.* **2012**, *51*, 7898–7921.
- (34) Stupp, S. I.; Palmer, L. C. Supramolecular Chemistry and Self-Assembly in Organic Materials Design. *Chem. Mater.* **2014**, *26*, 507–518.
- (35) Beaujuge, P. M.; Fréchet, J. M. J. Molecular design and ordering effects in π -functional materials for transistor and solar cell applications. *J. Am. Chem. Soc.* **2011**, *133*, 20009–20029.
- (36) Bates, F. S. Polymer-Polymer Phase Behavior. *Science* **1991**, *251*, 898–905.
- (37) Yassar, A.; Miozzo, L.; Gironda, R.; Horowitz, G. Rod–coil and all-conjugated block copolymers for photovoltaic applications. *Prog. Polym. Sci.* **2013**, *38*, 791–844.
- (38) Labastide, J. A.; Baghgar, M.; Dujovne, I.; Yang, Y.; Dinsmore, A. D.; Sumpter, B. G.; Venkataraman, D.; Barnes, M. D. Polymer nanoparticle superlattices for organic photovoltaic applications. *J. Phys. Chem. Lett.* **2011**, *2*, 3085–3091.
- (39) Labastide, J. A.; Baghgar, M.; Dujovne, I.; Venkataraman, B. H.; Ramsdell, D. C.; Venkataraman, D.; Barnes, M. D. Time- and Polarization-Resolved Photoluminescence of Individual Semicrystalline Polythiophene (P3HT) Nanoparticles. *J. Phys. Chem. Lett.* **2011**, *2*, 2089–2093.
- (40) Pauling, L. The Principles Determining the Structure of Complex Ionic Crystals. *J. Am. Chem. Soc.* **1929**, *51*, 1010–1026.
- (41) Bishop, K. J. M.; Wilmer, C. E.; Soh, S.; Grzybowski, B. A. Nanoscale forces and their uses in self-assembly. *Small* **2009**, *5*, 1600–1630.
- (42) Collier, C. P.; Vossmeier, T.; Heath, J. R. Nanocrystal superlattices. *Annu. Rev. Phys. Chem.* **1998**, *49*, 371–404.
- (43) Sanders, J.; Murray, M. Ordered arrangements of spheres of two different sizes in opal. *Nature* **1978**, *275*, 201–202.
- (44) Bartlett, P.; Ottewill, R. H.; Pusey, P. N. Superlattice formation in binary mixtures of hard-sphere colloids. *Phys. Rev. Lett.* **1992**, *68*, 3801–3804.

- (45) Gehan, T. S.; Bag, M.; Renna, L. A.; Shen, X.; Algaier, D. D.; Lahti, P. M.; Russell, T. P.; Venkataraman, D. Multiscale Active Layer Morphologies for Organic Photovoltaics Through Self-Assembly of Nanospheres. *Nano Lett.* **2014**, *14*, 5238–5243.
- (46) Potai, R.; Traiphol, R. Controlling chain organization and photophysical properties of conjugated polymer nanoparticles prepared by reprecipitation method: The effect of initial solvent. *J. Colloid Interface Sci.* **2013**, *403*, 58–66.
- (47) Almería, B.; Gomez, A. Electrospray synthesis of monodisperse polymer particles in a broad (60nm-2 μ m) diameter range: Guiding principles and formulation recipes. *J. Colloid Interface Sci.* **2014**, *417*, 121–130.
- (48) Horn, D.; Rieger, J. Organic Nanoparticles in the Aqueous Phase-Theory, Experiment, and Use. *Angew. Chemie Int. Ed.* **2001**, *40*, 4330–4361.
- (49) Kumar, P.; Mehta, A.; Mahurin, S. M.; Dai, S.; Dadmun, M. D.; Sumpter, B. G.; Barnes, M. D. Formation of oriented nanostructures from single molecules of conjugated polymers in microdroplets of solution: The role of solvent. *Macromolecules* **2004**, *37*, 6132–6140.
- (50) Maskey, S.; Osti, N. C.; Perahia, D.; Grest, G. S. Internal correlations and stability of polydots, soft conjugated polymeric nanoparticles. *ACS Macro Lett.* **2013**, *2*, 700–704.
- (51) Wang, J.-T.; Wang, J.; Han, J.-J. Fabrication of advanced particles and particle-based materials assisted by droplet-based microfluidics. *Small* **2011**, *7*, 1728–1754.
- (52) Landfester, K. Miniemulsions for Nanoparticle Synthesis. *Anion Sens.* **2003**, 75–123.
- (53) Kietzke, T.; Neher, D.; Landfester, K.; Montenegro, R.; Güntner, R.; Scherf, U. Novel approaches to polymer blends based on polymer nanoparticles. *Nat. Mater.* **2003**, *2*, 408–412.

CHAPTER 2

EFFECT OF FABRICATION PARAMETERS ON EXTERNAL CHARACTERISTICS OF P3HT NANOPARTICLES

2.1 Introduction

Given our modular approach to multi-length scale morphological control, it is crucial to have control of NP size, distribution in sizes, and particle stability. Many studies exist on how fabrication parameters affect nanoparticles when the polymer is synthesized in the miniemulsion.¹⁻³ However, at the start of this project not much was shown to optimize the method when using preformed conjugated polymers. Throughout the course of work on this thesis, multiple publications have emerged, on making nanoparticles of conjugated polymers.⁴

Fréchet and coworkers⁵ used a reprecipitation fabrication technique and investigated particle size dependence on physical properties of P3HT used, the synthetic method used to make P3HT, polymer's molecular weight, and regioregularity. They were able to produce particles ranging from 20nm-100nm in diameter and found that polymer concentration had the largest impact on NP size. Notably particle shape began to deviate from spherical shape utilizing high regioregular, synthesized by Grignard metathesis (GRIM). Belcher, et. al.⁶ fabricated particles of diameters 30nm and 130nm miniemulsion and reprecipitation, respectively with the aim to remove potentially charge-inhibiting surfactants.⁷ The result of most relevance to this chapter is the drastic change in

particle diameter when fabrication technique is changed. The full optimization of particle fabrication, keeping the fabrication method, polymer, and size characterization technique constant while also measuring dispersion stability remains unaddressed. This chapter aims to fill in this gap of knowledge.

Chapter 1 briefly explained our reasons for choosing the miniemulsion method for nanoparticle fabrication, potential control of solvent evaporation/solvent annealing of polymer in droplet, variety of parameters to tune for general use, and ability to scale-up. By understanding the underlying theory of miniemulsions, we can experimentally tune the fabrication to strategically vary the size of stable nanoparticles with a relatively narrow size distribution.

2.2 The Miniemulsion Method

In order to understand the miniemulsion method we must first define an emulsion. An emulsion is a colloidal dispersions of two immiscible liquids, droplets of liquid A (dispersed phase) are distributed in liquid B (continuous phase). Depending on the nature of A or B the emulsion can be defined as oil-in-water (O/W) or water-in-oil (W/O). Mini- comes from the droplet size range (1 μ m-100nm).

Input of energy is needed to create an emulsion, increasing the amount of interface between the immiscible liquids. If we disperse chloroform in water and stop the input of energy the phases will eventually separate to a single layer to minimize interfacial energy. There are two mechanisms responsible for

degradation, coalescence and Ostwald Ripening. Brownian motion helps to distribute droplets, however it can also result in collisions causing the droplets to coalesce. Droplets in a miniemulsion are also subject to Ostwald Ripening (mass transfer of dispersed phase of small to large droplets through the continuous phase).⁸ Therefore the fabrication of nanoparticles requires stabilization of the oil droplets to maintain a dispersed phase. Emulsions can be stabilized electrostatically or sterically by the use of surfactants. Since surfactants are amphiphilic (hydrophilic head group with hydrophobic tail), they can interact with both phases in an emulsion and will accumulate at the interface in order to minimize interfacial energy.⁹ Surfactant concentration is responsible for the droplet size in an emulsion, theoretically there is an equilibrium droplet size that can be stabilized by the amount of surfactant in the system.¹⁰

After creating the miniemulsion, the sample is heated to remove the liquid oil phase to leave an aqueous dispersion of NPs electrostatically stabilized by surfactant. This means ultimately the particle size comes down to the solid left in dispersion following evaporation of the oil phase. From all of that we can pull out the most important nanoparticle fabrication parameters in size, dispersity, and stability; 1) input of energy, 2) nature of oil droplet, 3) amount of surfactant, 4) solid content.

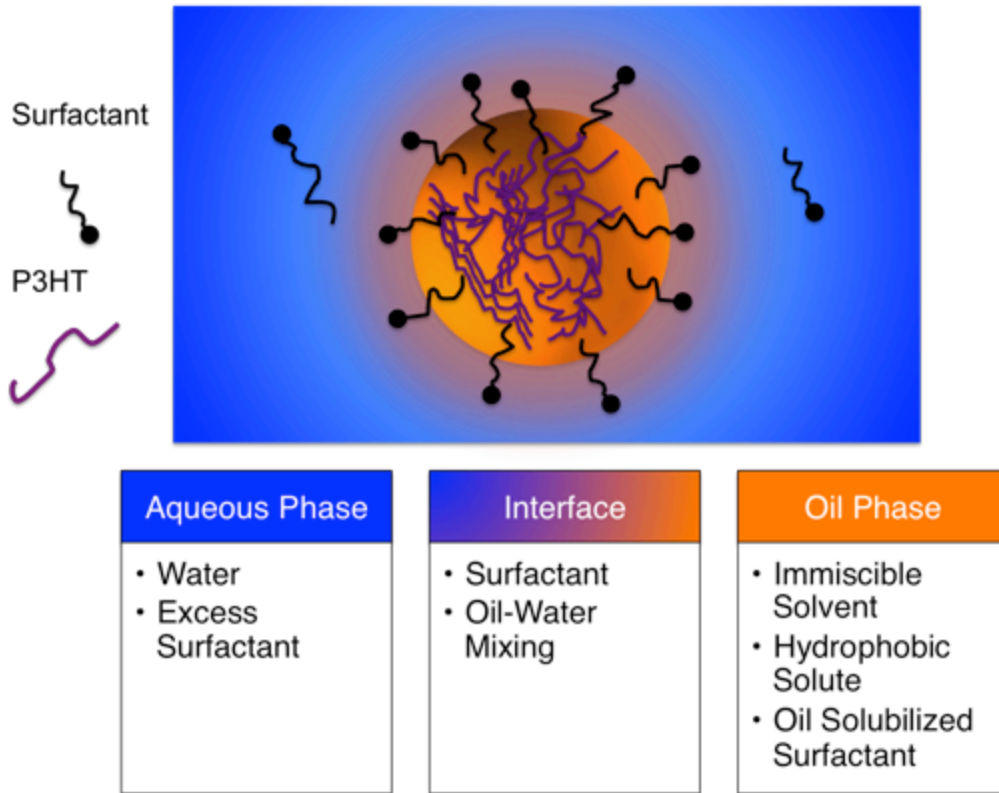


Figure 2.1: Cartoon of an enlarged emulsion droplet with phases and what is present.

2.3 Characterization Techniques

To examine the size and size distribution we use two main sizing techniques. At the start, we used a Malvern Nanosizer NS for dynamic light scattering (DLS) and more recently we have used a Nanosight NS500 for nanoparticle-tracking analysis (NTA). DLS detects the change in scattering intensity over time to calculate the Brownian motion of a particle in a medium of

known viscosity. The diffusion coefficient (D_t) can be directly correlated to the hydrodynamic diameter (D_h) of a sphere through the Stokes-Einstein equation,

$$D_h = \frac{k_B T}{3\pi\eta D_t}$$

where k_B is Boltzmann's constant, T is the temperature, η is the viscosity of the continuous phase. This technique limits the detectable size range, lower limitation is ability to scatter light, and upper limit is influenced by density because the motion is assumed to be Brownian motion and always assumes a spherical shaped particle. Because size is calculated from intensity of scattered light DLS results can over estimate the particle size as well as the ratio of particle sizes.¹¹ There is also an inherent error in the calculation of size distribution because it assumes a Gaussian type distribution.¹² One could utilize electron microscopy to measure size and size distribution of a sample, however the technique is time consuming and particles of the same size are known to segregate together¹³, possibly giving the false impression of narrow dispersity. All particle diameters in this chapter will be reported as Z-average, which is the intensity-weighted mean diameter as determined from cumulants analysis as defined in the International Standard on Dynamic Light Scattering ISO13321, ISO22142.

NTA, a more recent technology, visualizes the scattering of particles and from video data can tag and track specific particles allowing for a more accurate measurement of size distribution. Although the overall size calculation still

assumes a spherical particle, qualitatively this method allows visual detection of possible anisotropic particle shapes due to blinking of the tracked particle. This blinking is due to the inherent symmetry of scattering difference in the tumbling of a rectangular prism rather than an isotropic particle.

Stability of a NP sample is defined by the colloidal dispersions' ability to remain dispersed over time. In our case stability is very important for the assembly of nanoparticles and the scalability of the process as a whole. The idea of particle stability in a colloidal suspension is based on a theory developed Derjaguin, Landau, Verwey, and Overbeek in the 1940s^{14,15} DLVO theory relates particle stability to the total potential energy of the dispersion and is majorly dependent on the balance of attractive and repulsive van der Waals forces. As long as repulsive forces are dominant, particles resist flocculation and the dispersion is stable. Surfactant used in our NP fabrication generally provides sufficient electrostatic repulsion between particles. In order to quantify the stability we used electrophoretic mobility measurements to estimate the average zeta potential of particles in suspension. This technique applies a potential to the sample and utilizes the same principles as DLS to calculate the velocity of the particles in water under a known electric field. The zeta potential (ζ) is related to the electrophoretic mobility (μ_E) by the Henry Equation,

$$\mu_E = \frac{2\varepsilon\zeta F(ka)}{3\eta}$$

where, ϵ is the dielectric constant, ζ , is the zeta potential, $F(ka)$ is Henry's function and η is viscosity. Henry's function, the ratio of particle radius, a to the thickness of electric double layer, k , is estimated as 1.5 in polar medium using the Smoluchowski approximation. Colloidal suspensions in water are declared stable if the zeta potential is determined to be larger in magnitude than $\pm 25\text{mV}$ (kT/e).

2.4 Fabrication Optimization

Our general protocol to fabricate nanoparticles utilizes aqueous solution of sodium dodecyl sulfate (SDS) and a chloroform solution of P3HT. The chloroform solution is injected into the aqueous solution and then it is ultrasonicated. Following sonication the sample is stirred at $\sim 85^\circ\text{C}$ to evaporate CHCl_3 . P3HT used in these experiments was purchased from Rieke Metals $M_w=22\text{kDa}$ $\text{Đ}=2.13$ and $\text{RR}=90\text{-}93\%$ For specific experimental details see the appendix. All size and dispersity measurements in this chapter came from DLS. We first need to optimize the fabrication while keeping the emulsion composition constant. We can focus on the input energy and fabrication procedure.

2.4.1 Sonication Time And Power

To ensure sufficient input energy the sonication time and percent amplitude was varied. We hypothesized that by sonicating for longer times or increasing the power of the sonication the oil droplets would be further dispersed and yield a decrease in particle size. This also has the potential to affect the size

distribution by ensuring the equilibrium, stable, droplet size we might get more uniform particles.

Sonication times of 2, 5, and 15 minutes yielded NPs with diameter of 68 ± 13 nm, 58 ± 12 nm, and 57 ± 12 nm respectively (Figure 2.2). The error comes from the peak width obtained from DLS. Notably the 15-minute sample was hot to the touch after sonication and the sample had partially turned from orange to purple (a sign of solid state P3HT).

We also varied the percent maximum amplitude (Figure 2.3) from 10-50% and obtained particles of 50 ± 16 nm, 53 ± 12 nm, 51 ± 12 nm, 53 ± 12 nm, 52 ± 12 nm respectively. Upon observing no significant change in size or size distribution we concluded the ultrasonicator provided more than sufficient force to break up the emulsion and could in turn cause the oil phase to flash off quickly.

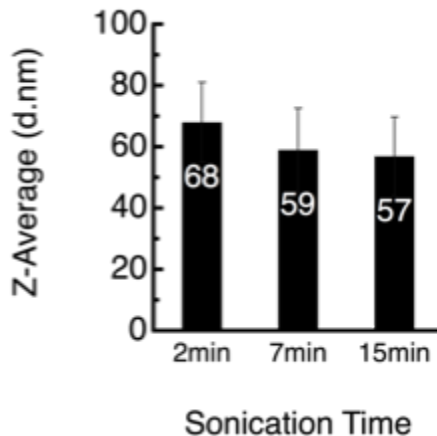


Figure 2.2: Diameter of P3HT NPs with increasing sonication time. Error bars represent the size distribution as half the Z-average peak width.

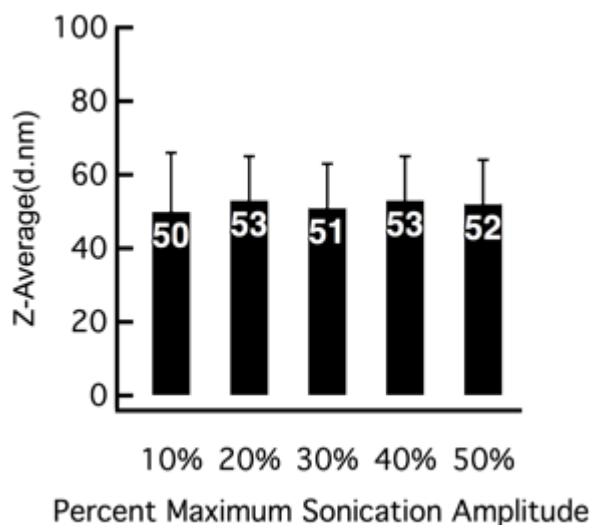


Figure 2.3: Diameter of P3HT NPs with increasing sonication power. Error bars represent the distribution as half the Z-average peak width.

2.4.2 Surfactant Concentration

Next, we wanted to vary parameters of the emulsion make up. Surfactant concentration can influence the stability of the emulsion. A higher concentration of surfactant can stabilize more interface, i.e. keep smaller droplets from coalescing. In theory, a larger amount of surfactant should give smaller nanoparticles until the droplets are sufficiently protected, any excess surfactant beyond this point should have no effect on size. Investigating a range of SDS concentrations, 0.2mM, 1mM, 4mM, 8.2mM, 12mM, 16mM, and 30mM, at low concentration of SDS particles of ~90nm are made and that can be reduced to 50nm by using a high concentration of SDS and this size within standard deviation plateaus above 16mM (Figure 2.4). These results agree with previous literature and we now have a known range of sizes to work with. It is worth mentioning that at high concentrations of SDS (above cmc 8.2 mM) the

temperature of the lab can cause clouding of the solution. We found measuring size was affected by the excess scattering.

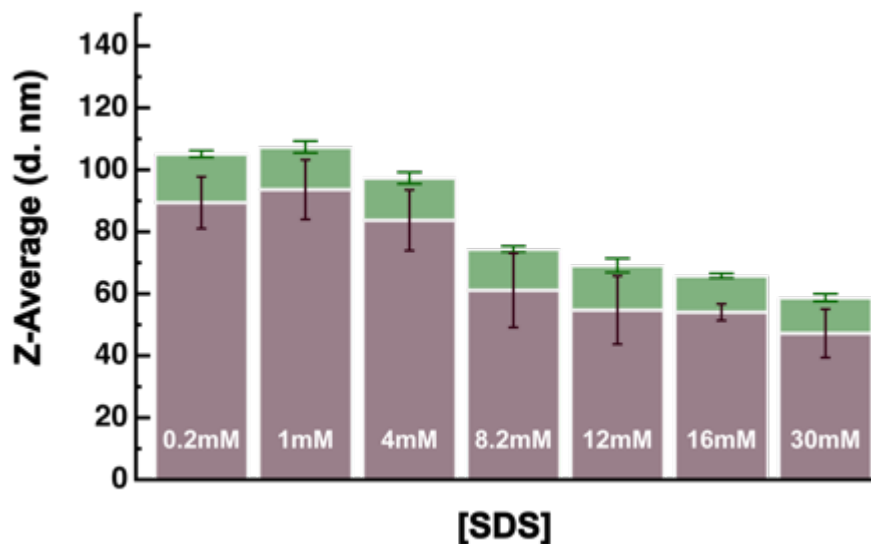


Figure 2.4: Diameter of P3HT NPs made with increasing surfactant concentration. Purple is Z-average, and green is the size distribution determined by the Z-average peak width. Error Bars are Standard deviation.

In order to insure accurate measurements on either end a series of dilutions were done and measured by DLS to compare size results. Aliquots from the same sample were diluted by water and by SDS solution. Within the range measured water dilution has negligible effect on the size calculation and as the sample is diluted with SDS solution the Z-average increases. We attribute this to excess scattering that skews the results.

2.4.3 Polymer Concentration

Polymer concentration has the largest effect on size meaning that the emulsion produces the same number of droplets with the polymer distributed between and as solvent evaporates, shrinks down to whatever solids are in the system. Sizes ranging from 40 nm (lowest wt%) to 120 nm (highest wt%) were obtained with fairly constant dispersity.

In the polymer concentration studies the particle size did not plateau within the range studied. The particles should continue to get smaller with fewer polymers contained in an emulsion droplet, until there is a single polymer chain, while increasing concentration should continue to grow the particles in size.

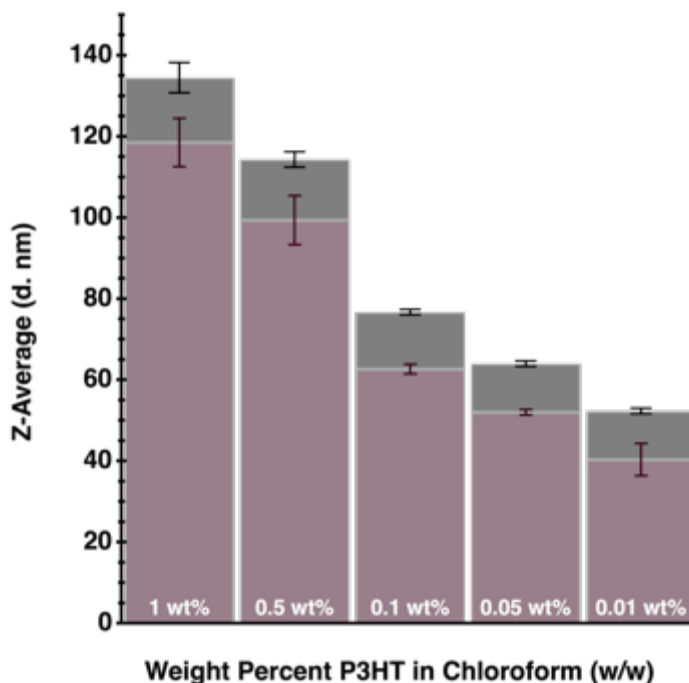


Figure 2.5: Diameter of P3HT NPs made with increasing P3HT concentration. Purple is Z-average, and grey is the size distribution determined by the Z-average peak width. Error Bars are Standard deviation.

To address stability we measured the size over time to detect any flocculation and took electrophoretic mobility measurements in order to calculate the zeta potential of our dispersions. Based on varying the surfactant concentration the NPs show a highly negative ZP of -60-70mV that is well below the needed thermal stability of -25mV. This was also confirmed by looking at size change of particles over periods of time.

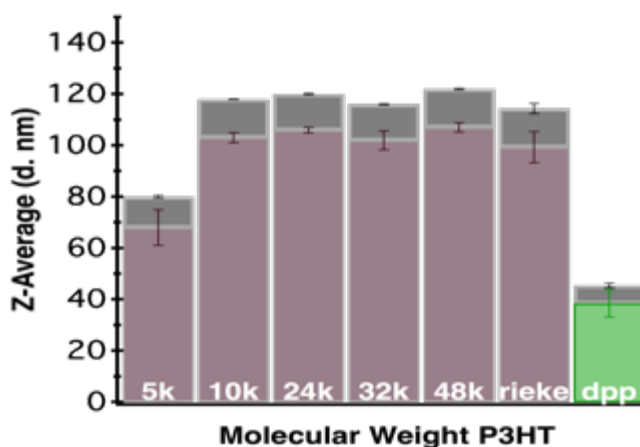


Figure 2.6: Diameter of polymer nanoparticles of varying molecular weight
The polymers used in these experiments were synthesized by Dr. Feng Liu

2.4.4 Nature Of Polymer

We also wanted to know if the method was applicable to various polymers and if the molecular weight and/or dispersity of polymer chain length would have any effect on the size or distribution.¹⁶ We made NPs with the same surfactant and polymer concentration varying the molecular weight of the P3HT all with high

regioregularity and low polydispersity (Figure 2.6). Interestingly the NPs made with 5K have a much smaller diameter (~70 nm) than the other P3HT particles (~100 nm), however all particles have relatively the same electrophoretic mobility. We also made particles with a polymer less crystalline or rigid in nature than P3HT and at the same concentration obtained particles as small as ~40 nm.

These results tell us that, first, the rigidity of the polymer plays a role in the sizes obtainable. Rigidity can be related to the persistence length of a polymer, and for a chain length shorter than the persistence length the polymer essentially behaves as a rod, where longer chains (higher molecular weights) allow for more bending.¹⁷

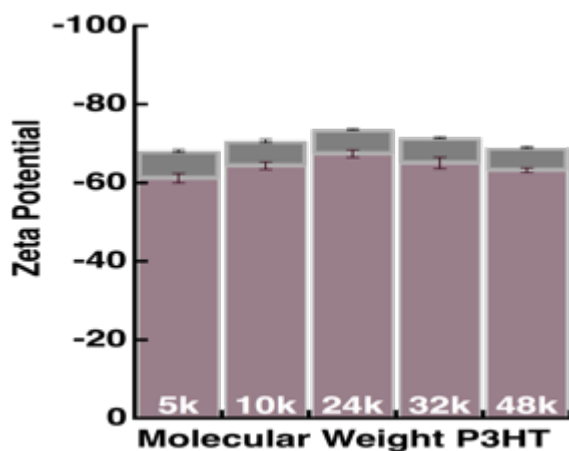


Figure 2.7: Zeta potential of P3HT particles made of various molecular weights. The polymers used in these experiments were synthesized by Dr. Feng Liu

2.5 Conclusion

Optimization of P3HT NP fabrication has given us a couple of pathways, surfactant concentration, polymer concentration, to tune the size of the particles

with the same relative size distribution. Increasing surfactant concentration causes a decrease in particle size, however the greatest range in size is afforded by varying the polymer concentration. The dispersions are electrostatically stable and the calculated Zeta Potential is independent of size pointing to an excess of surfactant in the final NP suspension. We have also shown that the nature of polymer (semicrystalline, rigid backbone or not) can influence the size range available, which begs for exploration of the polymer packing within a nanoparticle.

2.6 References

- (1) Landfester, K. Miniemulsions for Nanoparticle Synthesis. *Anion Sens.* **2003**, 75–123.
- (2) Schreiber, E.; Ziener, U.; Manzke, A.; Plettl, A.; Ziemann, P.; Landfester, K. Preparation of Narrowly Size Distributed Metal-Containing Polymer Latexes by Miniemulsion and Other Emulsion Techniques: Applications for Nanolithography. *Chem. Mater.* **2009**, 21, 1750–1760.
- (3) Chu, H.-H.; Hseih, R.-T. Effect of Surfactant Configurations on Miniemulsion Polymerization. *J. Macromol. Sci. Part A* **1995**, 32, 1353–1363.
- (4) Chen, J.-T.; Hsu, C.-S. Conjugated polymer nanostructures for organic solar cell applications. *Polym. Chem.* **2011**, 2, 2707.
- (5) Millstone, J. E.; Kavulak, D. F. J.; Woo, C. H.; Holcombe, T. W.; Westling, E. J.; Briseno, A. L.; Toney, M. F.; Fréchet, J. M. J. Synthesis, Properties, and Electronic Applications of Size-Controlled Poly(3-hexylthiophene) Nanoparticles. *Langmuir* **2010**, 26, 13056–13061.
- (6) Darwis, D.; Holmes, N.; Elkington, D.; David Kilcoyne, A. L.; Bryant, G.; Zhou, X.; Dastoor, P.; Belcher, W. Surfactant-free nanoparticulate organic photovoltaics. *Sol. Energy Mater. Sol. Cells* **2014**, 121, 99–107.
- (7) Bag, M.; Gehan, T. S.; Algaier, D. D.; Liu, F.; Nagarjuna, G.; Lahti, P. M.; Russell, T. P.; Venkataraman, D. Efficient charge transport in assemblies of surfactant-stabilized semiconducting nanoparticles. *Adv. Mater.* **2013**, 25, 6411–6415.
- (8) Landfester, K. Miniemulsion polymerization and the structure of polymer and hybrid nanoparticles. *Angew. Chemie Int. Ed.* **2009**, 48, 4488–4507.
- (9) Chen, Y. C.; Dimonie, V.; El-Aasser, M. S. Role of surfactant in composite latex particle morphology. *J. Appl. Polym. Sci.* **1992**, 45, 487–499.
- (10) Mason, T. G.; Wilking, J. N.; Meleson, K.; Chang, C. B.; Graves, S. M. Nanoemulsions: formation, structure, and physical properties. *J. Phys. Condens. Matter* **2006**, 18, R635–R666.
- (11) Zanetti-Ramos, B. G.; Fritzen-Garcia, M. B.; de Oliveira, C. S.; Pasa, A. A.; Soldi, V.; Borsali, R.; Creczynski-Pasa, T. B. Dynamic light scattering and

atomic force microscopy techniques for size determination of polyurethane nanoparticles. *Mater. Sci. Eng. C* **2009**, *29*, 638–640.

- (12) Patterson, J. P.; Robin, M. P.; Chassenieux, C.; Colombani, O.; O'Reilly, R. K. The analysis of solution self-assembled polymeric nanomaterials. *Chem. Soc. Rev.* **2014**, *43*, 2412–2425.
- (13) Wong, T.-S.; Chen, T.-H.; Shen, X.; Ho, C.-M. Nanochromatography Driven by the Coffee Ring Effect. *Anal. Chem.* **2011**, 11–13.
- (14) Derjaguin, B. On the repulsive forces between charged colloid particles and on the theory of slow coagulation and stability of lyophobic sols. *Transactions of the Faraday Society*, 1940, *35*, 203.
- (15) VERWEY, E. J. W. Theory of the stability of lyophobic colloids. *J. Phys. Colloid Chem.* **1947**, *51*, 631–636.
- (16) Koch, F. P. V.; Rivnay, J.; Foster, S.; Müller, C.; Downing, J. M.; Buchaca-Domingo, E.; Westacott, P.; Yu, L.; Yuan, M.; Baklar, M.; et al. The impact of molecular weight on microstructure and charge transport in semicrystalline polymer semiconductors—poly(3-hexylthiophene), a model study. *Prog. Polym. Sci.* **2013**, *38*, 1978–1989.
- (17) Baghgar, M.; Labastide, J. A.; Bokel, F.; Hayward, R. C.; Barnes, M. D. Effect of Polymer Chain Folding on the Transition from H- to J-Aggregate Behavior in P3HT Nanofibers. *J. Phys. Chem. C* **2014**, *118*, 2229–2235.

CHAPTER 3

EFFECT OF OIL PHASE ON THE INTERNAL STRUCTURE OF P3HT

NANOPARTICLES

3.1 Introduction

By creating a recipe to reliably tune the NPs external properties (Ch.2), we then turn our focus inward. The electronic properties of conjugated polymers are intimately related to their molecular packing thus the controlling the internal structure of P3HT NPs is of the utmost importance. We focused solely on NPs of P3HT for two reasons, 1) P3HT is OPV's archetypal hole conducting polymer¹ lending itself to an impressive amount literature on the structure property relationship data in thin films including processing conditions and polymer characteristics giving us a benchmark, 2) structural information can be obtained through absorption spectroscopy.

3.2 Aggregate Information From Absorbance

We used ultraviolet-visible absorption spectra (UV-vis) as a tool to monitor the changes in the polymer aggregation within the nanoparticle internal structure). To understand how to obtain structural information from optical spectroscopy let us start at the beginning of a conjugated molecule absorbing light. The process of light absorption causes an electron from the highest occupied molecular orbital (HOMO) to be promoted to the lowest unoccupied molecular orbital (LUMO). For a single molecule, these transitions are well

defined. Extension of orbital overlap via bonded conjugation introduces a band of states which overall lower the energetic gap between the HOMO and LUMO.

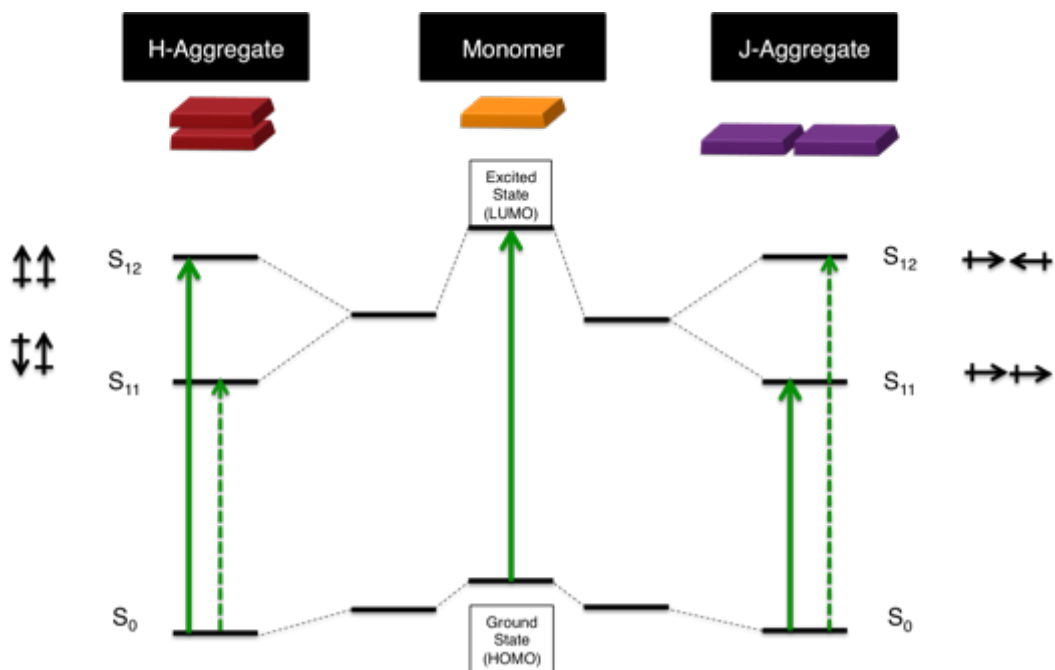


Figure 3.1: General energy diagram depicting the relative change in absorption due to transition dipole arrangement (black arrows) of dimeric identical chromophores. Recreated from discussions with Dr. Joelle Labastide and Professor Michael Barnes

As identical molecules come in close proximity, their transition-dipoles interact causing a split in degenerate energy levels and a change in absorption. The orientation of the dipoles to each other are elucidated in the wavelength of light absorbed. For example, when the chromophores are arranged in a face on overlap, or H-aggregate, the dipoles are side to side and split the LUMO into two states. (Figure 3.1) The parallel state is higher in energy due to repulsion, and therefore will have a high overall dipole moment and absorption. In contrast, the anti-parallel state results in a weaker absorption. This H-aggregate arrangement of chromophores results in a hypsochromic or blue shift in absorption. The

opposite occurs when the dipoles and chromophores are head to tail, or J-aggregate, the parallel state is lower in energy and has a higher overall transition dipole moment resulting in a bathochromic or red shift in absorption.

In the case of conjugated polymers, each monomer unit is a chromophore and can absorb light to reach their excited state. For P3HT, just like in other conjugated polymers, as the molecule moves from the ground state to the excited state there is a change in geometry. In the ground state, each thiophene unit is aromatic with double bonds alternated within the ring. When an electron is promoted to the first excited state (from the HOMO to the LUMO) the double bonds shift and the molecule adopts a quinoidal-like structure where there is a single double bond at the bottom of the ring and the bonds connecting 3-hexylthiophene units are now double bonds. This rearrangement of bonds means a shift in the electron density of the molecule, so the electronic excitation is coupled to a vibrational transition.

For a single P3HT molecule the vibronic progression in the absorption spectra is well defined, however when the P3HT chains are closely packed this electron-phonon coupling, becomes distorted due to the different aggregate states present. Spano and coworkers^{2,3} modeled the vibronic transitions using a Frank-Condon fit, under different coupling conditions to reproduce absorption spectra. The model presented gives us the ability to use absorption spectra to gain a general idea of the aggregate structure within a sample. (Figure 3.2)

For P3HT well dissolved in solution, we see an absorbance peak around 450nm (figure 3.3) from the purely amorphous polymer. The distinct difference in purely amorphous absorption and aggregate P3HT absorption gives us the ability to 1) obtain a relative ratio of amorphous to aggregate P3HT in a nanoparticle sample, 2) remove the amorphous contribution to look at only the changes absorption from aggregate P3HT.⁴

As stated above, P3HT undergoes a vinyl stretch when excited, this distortion in the molecule can cause vibrational excitations in its nearest neighbors. The vinyl stretch deviation can be related to change in UV spectra.

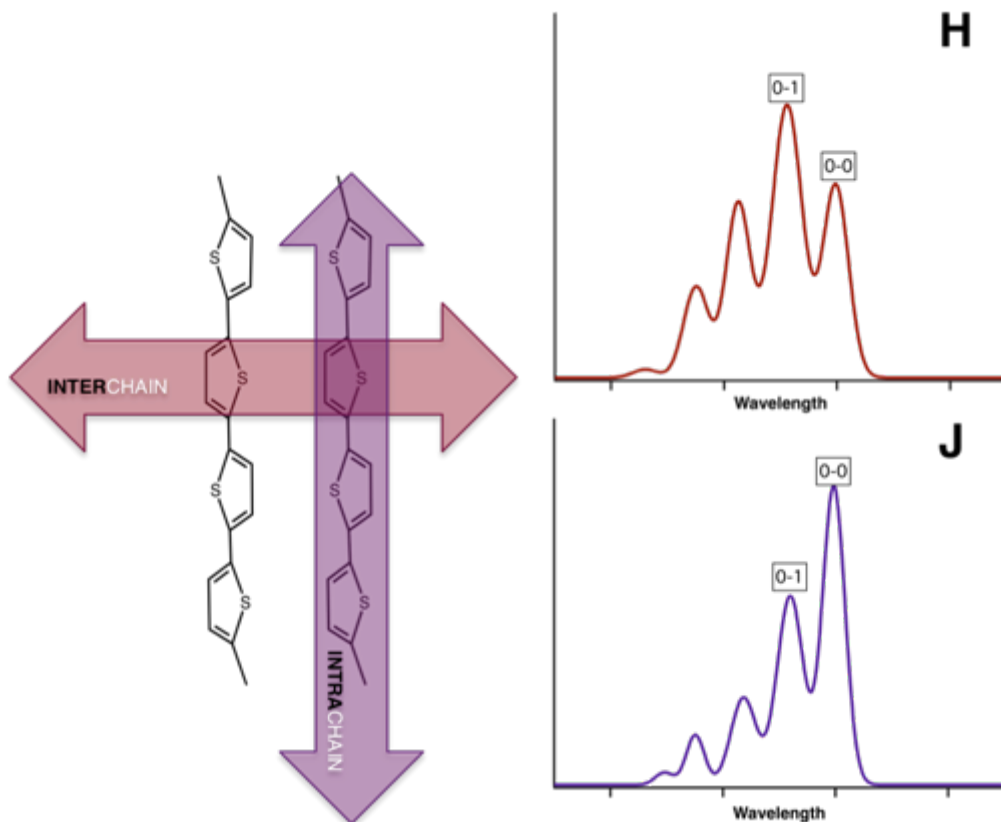


Figure 3.2: (left) Molecular depiction of thiophene packing with arrows in the direction of interchain (H-aggregate) and intrachain (J-aggregate) coupling. (right) Recreated absorption spectra of pure H and J aggregates of P3HT with 0-0 and 0-1 transition peaks labeled.

Based on Spano's H/J aggregate model⁵, we can estimate the degree of chromophore coupling along the polymer backbone (intrachain) and pi-pi stacking between chains coupling. From the intensity ratio of the 0-0 to 0-1 peaks in the absorption spectrum the nearest neighbor coupling, J_0 , can be found, the sign of which determines the H or J character of the aggregate.

$$\frac{A_{0-0}}{A_{0-1}} = \left(\frac{1 - 0.96J_0/\omega_0}{1 + 0.29J_0/\omega_0} \right)^2$$

Comparing nanoparticle samples of similar size and percent aggregate P3HT allows the analysis to focus on the nature of the aggregate. In general, a ratio of greater than 1 suggests a dominance of J-aggregates (intrachain coupling), and a ratio of less than 1 suggests a dominance of H-aggregates (interchain coupling).

3.3 Effect Of Solvent On Structure Of P3HT Thin Films

The solvent P3HT thin films are cast from is known to significantly affect the resulting structure due to the aggregate nature in solution.⁶⁻¹¹ For example in chloroform, a relatively good solvent for P3HT, the polymer is well solvated, as indicated in the purely amorphous absorbance. The resulting films have poor intrachain ordering. However, for films cast from P3HT in toluene the intrachain order is enhanced. Toluene is a marginal solvent for P3HT therefore the aggregation can begin in solution.^{8,12} We must keep in mind, that toluene has a

higher vapor pressure than chloroform that also affects the crystallization kinetics.

Clark and coworkers⁴ have shown that increasing the boiling point of the processing solvent continues to increase (decrease) the A_{0-0}/A_{0-1} peak ratio (exciton band width W), while also increasing the overall amount of aggregate P3HT as determined from the absorption spectra. We wanted to know if the same rules applied to making spherical NPs of P3HT. The packing of a rigid polymer that prefers a planar orientation into a spherical shape with the radius or even diameter comparable to the contour length (65nm for MW of 29K of P3HT, allows for exploration into confinement effects on the polymer.

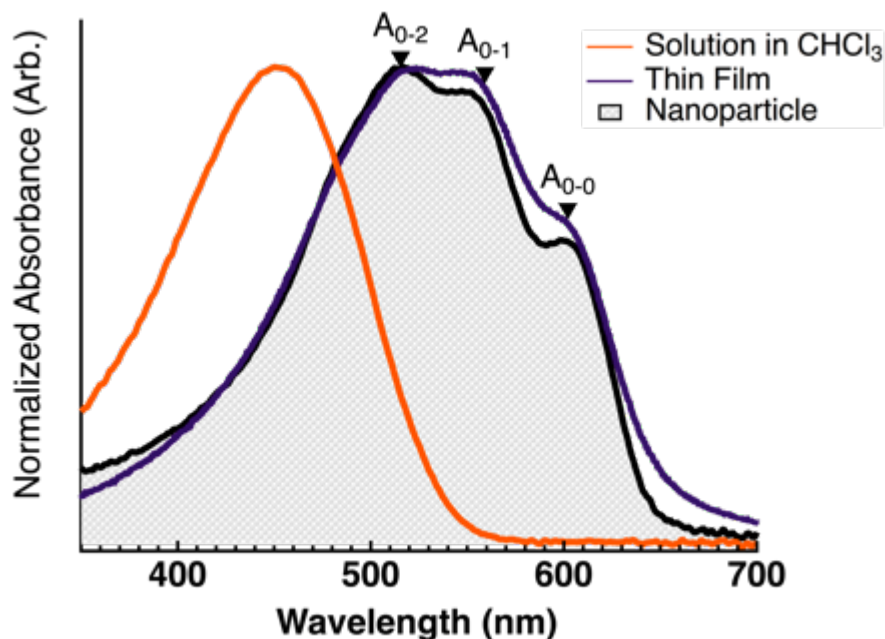


Figure 3.3: Absorption spectra of P3HT in chloroform (orange), spun cast thin film (purple) and nanoparticle dispersion (black filled) with peaks marked

3.4 Effect of Solvent on P3HT Nanoparticles

The miniemulsion technique was used to fabricate P3HT NPs from three solvent systems, chloroform, toluene and a mixture of CHCl_3 /toluene (1:4 v/v). 0.25mL of 0.5wt% (Rieke, MW=22kDa, D=2.13 RR=90-93%) of P3HT in oil was injected into a 20mL vial of 2.5mL of 1mM SDS in Nanopure water (spec). The mixture was emulsified using ultrasonication with a microtip for two minutes at 30% maximum amplitude (spec). The sample was then stirred at 80C for 15-60min depending on solvent boiling point. Following oil phase evaporation the sample was allowed to cool to room temperature then filtered through a 0.25um pore size syringe filter.

The first thing noticed is the size change from chloroform to toluene, 142nm to 124nm respectively with the mixed solvent right in the middle at 135nm. We see a similar trend for the A_{0-0}/A_{0-1} ratio where chloroform has the

Table 3.1: Size, A_{0-0}/A_{0-1} Intensity of P3HT Nanoparticles Synthesized from Different Solvent Composition^a

Solvent	Z (d.nm) ^a	A_{0-0}/A_{0-1} ^b
CHCl_3	142±15	0.71±0.05
Toluene/ CHCl_3 ^c	135±14	0.68±0.03
Toluene	124±13	0.66±0.05

^aMean of Z-average peak from several trials and the error is average of half-width of the peak. ^bMean of several trials and the error is standard deviation. ^cMixture of toluene and chloroform in 1:4 (v/v) ratio.

highest at 0.71, then mixed 0.68, then toluene 0.66. (Table 3.1) The percent aggregate versus amorphous as determined from the absorption remains relatively constant ~80% for all three solvents. However, the aggregate contribution to the spectrum seems to decrease with decreasing solvent quality, indicating a change in quantum yield. (Figure 3.4) These results imply that the nature of aggregate structure inside the nanoparticle is affected by solvent quality and appears to deviate from what is known in thin films.

The formation of a film and a nanoparticle differ in spatial constraints for polymer assembly, which we propose as a potential cause for deviation from aggregate structure due to solvent. We noticed a change in color of the P3HT dissolved in toluene over time from bright orange reddish-brown that is indicative of polymer aggregation. This occurred more rapidly for the marginal solvent toluene than our good solvent chloroform. In order to probe the P3HT aggregates formed in solution, before making nanoparticle we used UV to detect deviation from the amorphous P3HT absorption and performed dynamic light scattering to characterize aggregate size. (Figure 3.5) P3HT in toluene is the only sample with a large broad peak around 610nm at room temperature that disappears when the temperature is raised to 70°C. DLS results give particulate sizes of 16 nm for CHCl₃, 42 nm for mixed solvent and 219 nm for toluene. Based on absorption and DLS, the polymer is well dissolved in chloroform and mostly dissolved in the mixture of toluene/chloroform while it aggregates in toluene at room temperature.

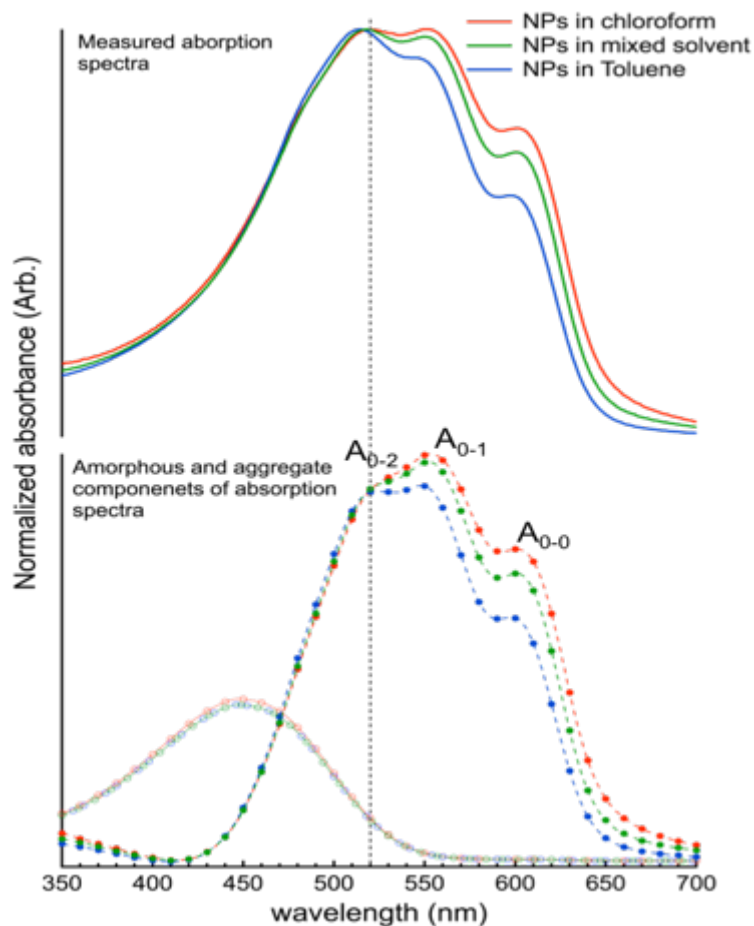


Figure 3.4: (top) Normalized absorption spectra of P3HT nanoparticles made from chloroform, toluene, and 1:4 mixture of toluene to chloroform. (bottom) open-circle line and closed-circle line show the amorphous absorption and aggregate absorption respectively in each nanoparticle spectra. Vertical dashed line indicates the A_{0-2} peak position (520 nm) and separates the solvent-quality independent part of the absorption spectra from the region that is fairly affected by solvent. Reprinted from reference 13.

In the miniemulsion fabrication process, the evaporation temperature is 80°C causing the chloroform to quickly flash off as evidenced by a quick color change of the dispersion from orange to purple. The chains are kinetically trapped in random conformations leading to a greater dispersity in aggregates and a larger particle diameter. In contrast, the polymer is less soluble in toluene, and starts to aggregate before all the solvent is removed. These aggregates can

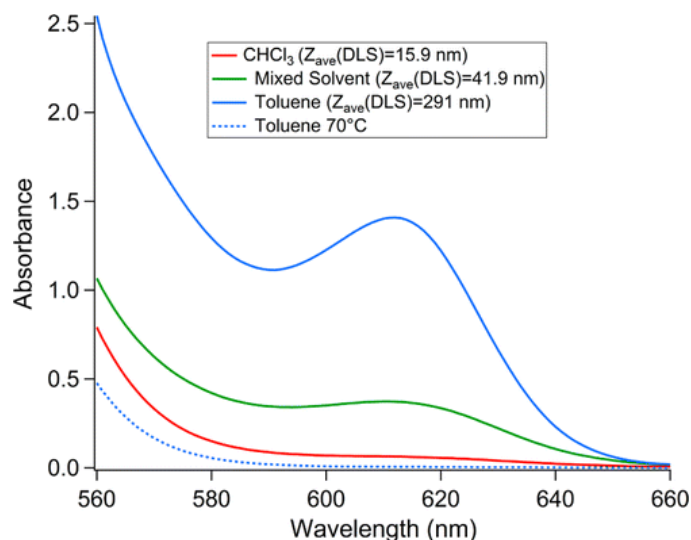


Figure 3.5: UV-vis absorption spectra of P3HT in various solvents. The presence of a peak around 610 nm indicates the presence of P3HT aggregates. The sizes of the P3HT aggregates measured by dynamic light scattering of 0.5 wt % P3HT solution in different solvents are shown in the figure key. For clarity absorption spectra is shown between 560 and 660 nm. Reprinted from Reference 13.

be annealed due to a slower evaporation rate of toluene leading to overall tighter packing of polymer chains, supported by a smaller particle size. The NPs made from toluene also have a similar dispersity in aggregate nature as CHCl_3 NPs. As the toluene, already a marginal solvent, is evaporated the concentration of P3HT continues to increase while decreasing solubility. The decreased solubility limits the polymer chain mobility, potentially leaving a distribution of partially annealed aggregates. The mixture of CHCl_3 and Toluene (mixed solvent) appears to take the best of both worlds by landing in the middle of size and peak ratio with a narrow distribution. The results can be explained by high chain mobility in a good solvent, chcl3 , and extended time to order the chains with toluene present.

UV-Vis spectroscopy, being a bulk measurement, can give an important but limited picture of nanoparticle dispersions. Therefore, time-resolved photoluminescence (TRPL) measurements on single particles were collected by Dr. Joelle Labastide to provide further insight to the aggregate nature within the particle.^{14,13,15} In figure 3.6, the range of fast time component is plotted by the range of the slow time component to highlight the distribution in lifetimes. The distribution of the decay lifetimes indicates inhomogeneity of the aggregate structure. For single solvent systems, we see nearly double the width in distribution versus the nanoparticles made with the mixed solvent. These results correlate well with the UV-Vis data, point to a more uniform aggregate structure obtained when using a mixture of good and marginal solvent.

Nanoparticles were made using a lower evaporation temperature (60°C) to better distinguish the effect solvent evaporation rate from aggregates pre-formed in solution. The absorbance spectrum of the low temp particles made from chloroform appears to reproduce the characteristics of the particles made with mixed solvent.

However, TRPL results indicate (Fig 3.6) a significant difference in lifetimes, with a longer fast component and shorter slow component. This implies that the slow evaporation rate of toluene is not solely responsible for the internal structure of NPs made from the mixed solvent system.

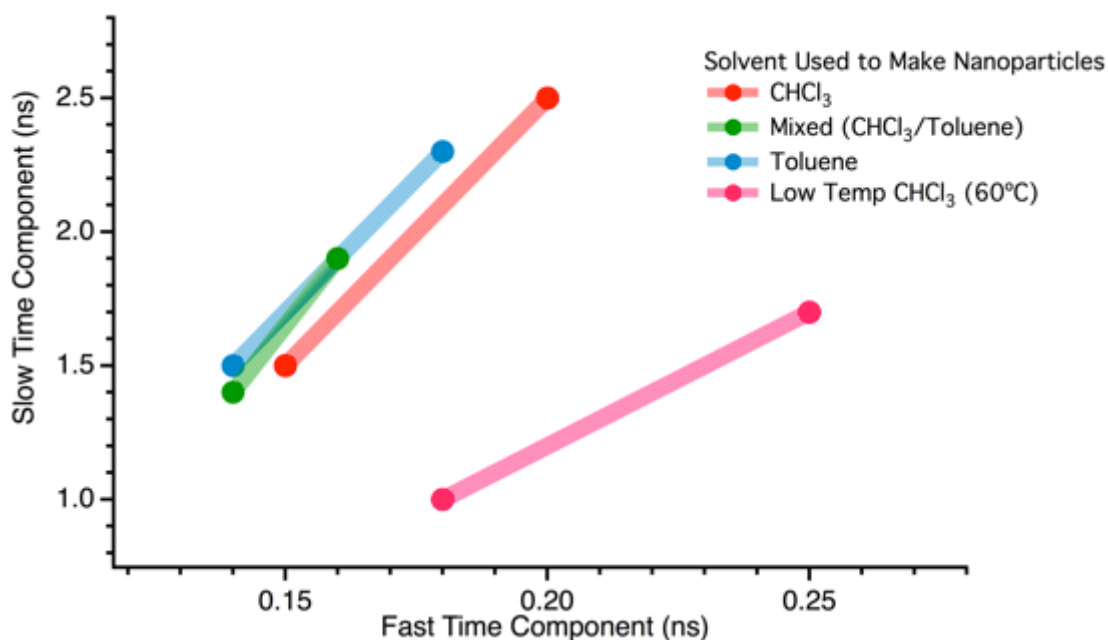


Figure 3.6: Recreated from TRPL results on single nanoparticles from reference 13. The range of slow time component is plotted by fast time component from nanoparticles made from various solvents and lowering the evaporation temperature.

3.5 Conclusion

In summary, we have show that the oil phase is a powerful knob to tune the aggregation of P3HT within the nanoparticles. We find that using a solvent mixture of a good solvent a marginal solvent provides structurally ordered P3HT aggregates within nanoparticles. We also find that the influence of solvent on the nature of P3HT aggregation within nanoparticles is different from the solvent influence seen in thin films; most notably evidence by the constant amount of aggregated P3HT chains with varying absorption spectra.

3.6 References

- (1) Dang, M. T.; Hirsch, L.; Wantz, G. P3HT:PCBM, Best Seller in Polymer Photovoltaic Research. *Adv. Mater.* **2011**, *23*, 3597–3602.
- (2) Spano, F. C. Modeling disorder in polymer aggregates: The optical spectroscopy of regioregular poly(3-hexylthiophene) thin films. *J. Chem. Phys.* **2005**, *122*, 234701.
- (3) Spano, F. C. Absorption in regio-regular poly(3-hexyl)thiophene thin films: Fermi resonances, interband coupling and disorder. *Chem. Phys.* **2006**, *325*, 22–35.
- (4) Clark, J.; Chang, J. F.; Spano, F. C.; Friend, R. H.; Silva, C. Determining exciton bandwidth and film microstructure in polythiophene films using linear absorption spectroscopy. *Appl. Phys. Lett.* **2009**, *94*, 163306–1 – 3.
- (5) Spano, F. C. The spectral signatures of frenkel polarons in H- And J-aggregates. *Acc. Chem. Res.* **2010**, *43*, 429–439.
- (6) Scharsich, C.; Lohwasser, R. H.; Sommer, M.; Asawapirom, U.; Scherf, U.; Thelakkat, M.; Neher, D.; Köhler, A. Control of aggregate formation in poly(3-hexylthiophene) by solvent, molecular weight, and synthetic method. *J. Polym. Sci. Part B Polym. Phys.* **2012**, *50*, 442–453.
- (7) Wang, T.; Dunbar, A. D. F.; Staniec, P. A.; Pearson, A. J.; Hopkinson, P. E.; MacDonald, J. E.; Lilliu, S.; Pizzey, C.; Terrill, N. J.; Donald, A. M.; et al. The development of nanoscale morphology in polymer:fullerene photovoltaic blends during solvent casting. *Soft Matter* **2010**, *6*, 4128.
- (8) Xue, L.; Gao, X.; Zhao, K.; Liu, J.; Yu, X.; Han, Y. The formation of different structures of poly(3-hexylthiophene) film on a patterned substrate by dip coating from aged solution. *Nanotechnology* **2010**, *21*, 145303.
- (9) Machui, F.; Langner, S.; Zhu, X.; Abbott, S.; Brabec, C. J. Determination of the P3HT:PCBM solubility parameters via a binary solvent gradient method: Impact of solubility on the photovoltaic performance. *Sol. Energy Mater. Sol. Cells* **2012**, *100*, 138–146.
- (10) Johnson, C. E.; Boucher, D. S. Poly(3-hexylthiophene) aggregate formation in binary solvent mixtures: An excitonic coupling analysis. *J. Polym. Sci. Part B Polym. Phys.* **2014**, *52*, 526–538.

- (11) Hu, S.; Dyck, O.; Chen, H.; Hsiao, Y.; Hu, B.; Duscher, G.; Dadmun, M.; Khomami, B. The impact of selective solvents on the evolution of structure and function in solvent annealed organic photovoltaics. *RSC Adv.* **2014**, *4*, 27931.
- (12) Chen, P.-Y.; Rassamesard, A.; Chen, H.-L.; Chen, S.-A. Conformation and Fluorescence Property of Poly(3-hexylthiophene) Isolated Chains Studied by Single Molecule Spectroscopy: Effects of Solvent Quality and Regioregularity. *Macromolecules* **2013**.
- (13) Nagarjuna, G.; Baghgar, M.; Labastide, J. A.; Algaier, D. D.; Barnes, M. D.; Venkataraman, D. Tuning aggregation of poly(3-hexylthiophene) within nanoparticles. *ACS Nano* **2012**, *6*, 10750–10758.
- (14) Labastide, J. A.; Baghgar, M.; Dujovne, I.; Venkataraman, B. H.; Ramsdell, D. C.; Venkataraman, D.; Barnes, M. D. Time- and Polarization-Resolved Photoluminescence of Individual Semicrystalline Polythiophene (P3HT) Nanoparticles. *J. Phys. Chem. Lett.* **2011**, *2*, 2089–2093.
- (15) Labastide, J. A.; Baghgar, M.; McKenna, A.; Barnes, M. D. Time- and Polarization-Resolved Photoluminescence Decay from Isolated Polythiophene (P3HT) Nanofibers. *J. Phys. Chem. C* **2012**, *116*, 23803–23811.

CHAPTER 4

EFFECT OF SURFACTANT ON THE INTERNAL STRUCTURE OF P3HT NANOPARTICLES

4.1 Introduction

Following the study of changing solvent quality for P3HT in the miniemulsion, we were interested in using the method of making NPs on any semiconducting polymer. We are interested in understanding what other aspects can be generally applied to any system. Based on the nature of a miniemulsion (Figure 2.1) the surfactant has the most potential to affect molecular packing. We recognized small molecule amphiphiles can hypothetically be present in the aqueous phase at the interface and in the oil phase. Surfactant effect was hinted at in early work when sodium dodecyl sulfate (SDS) was swapped with cetyltrimethylammonium bromide (CTAB). Figure 4.1 shows the surfactant structures and absorption spectra of P3HT NPs made with either SDS or CTAB. The samples made with CTAB show a slight blue shift and a large decrease in

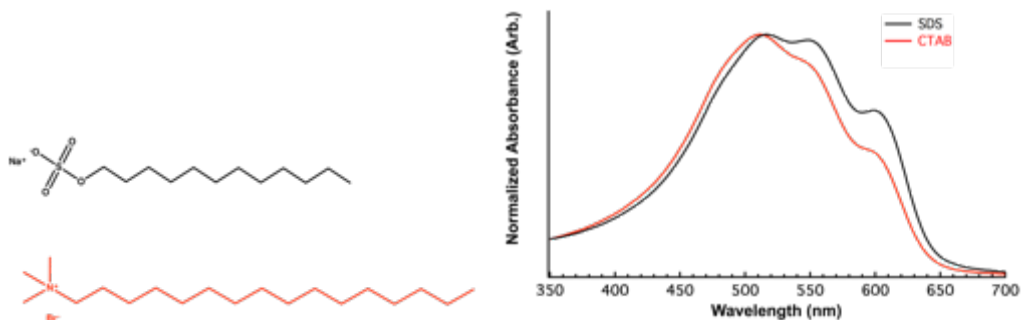


Figure 4.1: Molecular structures and absorbance of nanoparticles made with sodium dodecyl sulfate (SDS in black) and cetyltrimethylammonium bromide (CTAB in red)

aggregate absorption.

We want to probe this idea further to lay the groundwork for a broadly applicable method of fabricating nanodomains with a desired property due to molecular packing. To start with, we thought about the possible ways surfactant could affect P3HT NPs and what those results would look like; 1) direct interaction with P3HT chains via the interface directing the packing and promoting nucleation, 2) oil phase soluble surfactant interfering or enhancing P3HT aggregate assembly, 3) Interfacial coverage could vary with surfactant allowing oil and water to mix and ultimately precipitate the P3HT 4) As seen in in-situ synthesis of polymer in emulsion the surfactant can template the nanoparticle shape.¹⁻⁵ The absorption spectra is our main marker of the nature of P3HT aggregate in the NPs, specifically the ratio of the A_{0-0}/A_{0-1} peaks, the amount of

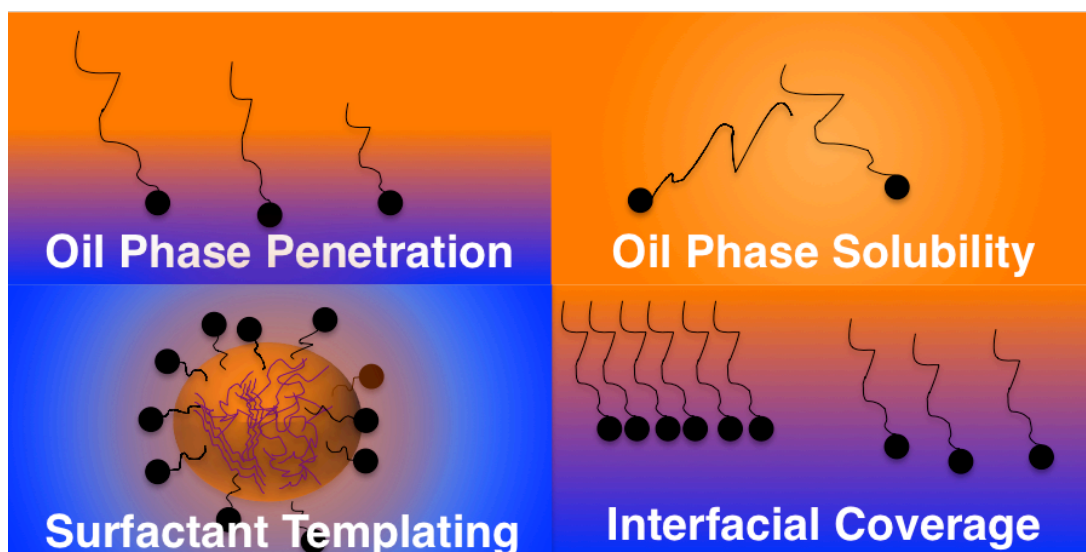


Figure 4.2: Possible scenarios for surfactant to affect the internal structure of the nanoparticle.

aggregate versus amorphous absorption signal, and the peak positions.

A paper was recently published looking at the influence polymeric surfactants on the UV-Vis absorption spectra of P3HT nanoparticles. Fleischli and coworkers⁶ used two block-copolymer surfactants with one block n-Butyl methacrylate (BuMA) with the other block being Poly(ethylene glycol) methacrylate (PEGMA) or 2-(Dimethylamino) ethyl methacrylate (DMAEMA) as their emulsifiers. Although the surfactants were primary the study also varied oil phase, phase the surfactant was dissolved in, processing temperature and processing type. The P3HT particles made ranged in size from 60nm-400nm and the size did not seem to correlate with the absorption spectra obtained. One significant change in peak ratio comes from the type of processing of emulsions, mechanical stirring afforded a more pronounced A_{0-0} peak as opposed to ultrasonication. The other main factor was the processing temperature where the particles made with DMAEMA containing surfactant, known to be temperature sensitive, showed more J-like absorbance when processed as 80°C versus room temperature. Nanoparticle made with PEGMA containing surfactant, not temperature sensitive, showed no significant change due to processing temperature. This study further supports the potential of surfactants influencing the aggregate structure in P3HT nanoparticles, and gives a view into the complexity of polymer nanoparticles made via emulsion.

4.2 Anionic Surfactant Chainlength

This section will focus on the possible amount of surfactant tail penetrating the oil phase, and either directing packing or changing solubility of P3HT in the system. The hydrocarbon chainlength of a surfactant is varied while keeping the headgroup constant. Starting with the surfactant we have the most experience with, SDS. There are commercially available sodium sulfate linear hydrocarbons with chainlengths of 8, 12, 14, 18 carbons. The number of carbons translates to hydrocarbon chain lengths from roughly 0.8nm to 2nm. Longer tails could further penetrate the oil phase therefore increasing the possibility of intermolecular interaction. This hypothesis is reasonable because of the log P, related to the partitioning into octanol over water, increased for linear alkanes and their carboxylic acid derivatives. (Table 4.1)

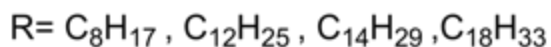
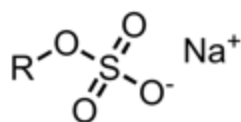
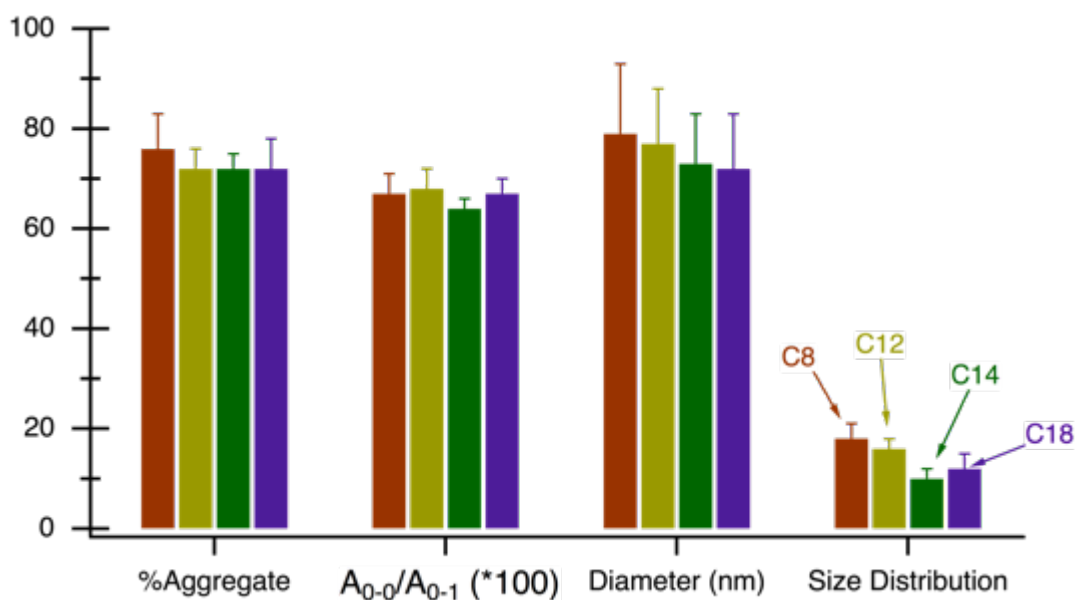


Figure 4.3: Sodium sulfate surfactant head group with a series of linear

Linear Alkanes	Log P	Carboxylic Acids	Log P
C ₈ H ₁₈	5.15	C ₈ H ₁₆ O ₂	3.05
C ₁₀ H ₂₂	6.25	C ₁₀ H ₂₀ O ₂	4.09
C ₁₂ H ₂₆	6.80	C ₁₂ H ₂₄ O ₂	4.6
C ₁₄ H ₃₀	8.00	C ₁₄ H ₂₈ O ₂	6.1
		C ₁₆ H ₃₂ O ₂	7.17

As shown in Figure 4.4 the particle size, size distribution, %aggregate and peak ratio stays relatively constant for all chain lengths. The lack of surfactant chain length affecting internal packing is interpreted as, the polymer aggregation must occur from inside the oil droplet. By DLS, we measured droplet size to be on the order of microns, therefore the surfactant tail (longest 2nm) would not direct the polymer packing.

However as mentioned previously the chloroform can flash off quite quickly so we lowered the evaporation temperature to slow the process. This should also affect the diffusion of the surfactants, overall increasing possible interaction.



**Figure 4.4: Comparison of percent aggregate and peak ratio* as determined by UV-vis absorbance, and size characteristics of P3HT nanoparticles made with sodium sulfate head group surfactants with varying length of hydrocarbon tail C8 (red), C12 (yellow), C14 (green) C18(purple). Error bars represent standard deviation
* peak ratio is multiplied by 100 for visibility on the plot**

4.2.1 Temperature

The evaporation temperature varied at 80, 40, and 20°C. The lowest temperature caused C18 to make the solution cloudy. The samples were heated until clear in order to avoid scattering from surfactant in the absorbance measurement. Note that the scattering affected only the amorphous section the spectra, by heating, there was no change in the relative A_{0-0} to A_{0-1} peaks. As seen in the spectrum (Figure 4.5) there is no significant change for C8 or C12 samples, however C18 has a noticeable increase in intrachain ordering and a red shift of a couple nanometers when the evaporation temperature is lowered.

At concentrations of 1 mM the orange to purple color-change was noticed during sonication. There are two reasons for the polymer to aggregate, first the sonication can produce a large amount of heat affecting the chloroform if the droplets are not well covered and second ultrasonication is known to induce polymer aggregation in solution. If the polymer aggregate structure is set during sonication then the surfactant has no chance influencing the P3HT packing. Therefore, we propose the need for better droplet protection through increasing the concentration of surfactant to fully cover the oil-water interface.

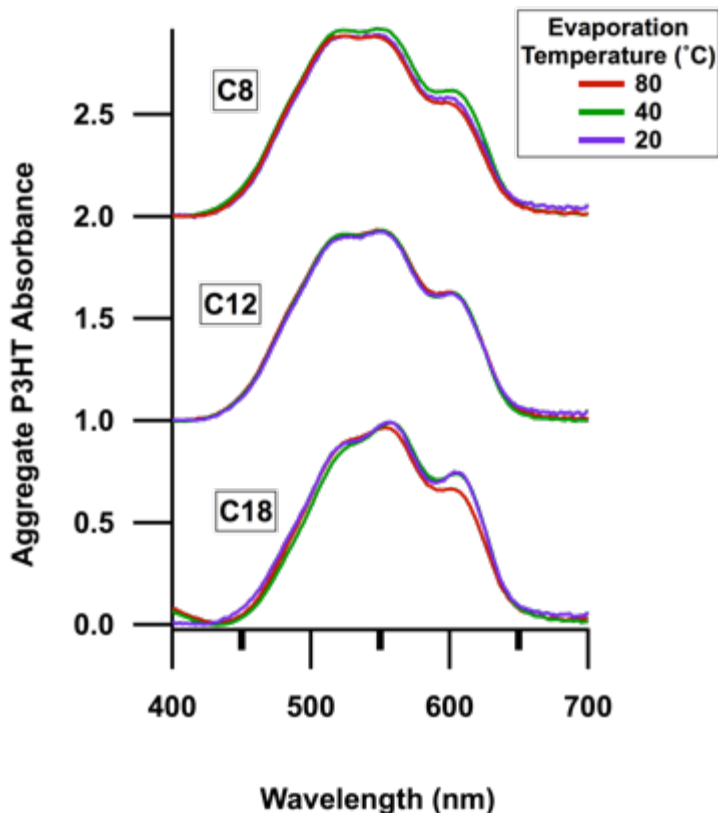


Figure 4.5: UV absorbance of C8, C12, C18 SDS surfactants with varying evaporation temperature

4.2.2 Concentration

To push C18 to its maximum possible effect we increased the concentration from 1mM to 10mM while keeping the evaporation temperature at 20°C (Figure 4.6). It is known that the surfactant tails will straighten out, in effect penetrating the droplet further when there is a higher amount of surfactant at the interface.⁷

The particle size dropped to ~50 nm at high concentration. Similar to the temperature study, the internal structure of NP samples made with shorter

surfactant chains, C8 and C12, is relatively unaffected. However, C18 reverts to a lower A_{0-0}/A_{0-1} ratio and A_{0-0} peak is blue shifted by 4nm.

Overall, C18 seems to have minor influence but is extremely limited in the range of aggregate nature. Therefore, we can conclude that linear alkyl hydrocarbons with sodium sulfate head groups do not influence the P3HT aggregate structure within a nanoparticle. However as previously mentioned (Figure 4.1) there is a noticeable change from P3HT NPs made with SDS to NPs made with CTAB, this phenomenon is probed further in the following section.

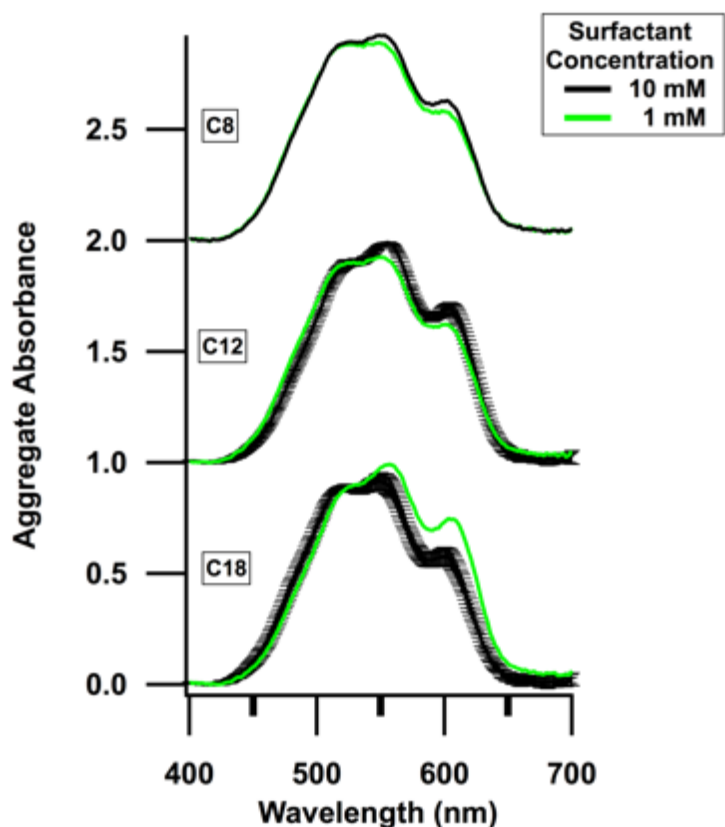


Figure 4.6: UV-Vis absorbance of P3HT nanoparticles made with 10 mM (black) and 1 mM (green) surfactant concentration of C8, C12, C18 Chainlengths.

4.3 Cationic Surfactant Chainlength

Because of the change in aggregate structure from SDS to CTAB we were curious as to how the headgroup, or the charge on the surfactant could possibly play a role in P3HT aggregate structure. We first looked at a small chainlength series, C12, C14, C16 and before filtration there is a direct trend of peak ratio to chain length. With decreasing alkyl chain length, we see a red shift in the A_{0-0} peak and simultaneously increase in intensity. However, once the samples were filtered with a $0.45\mu\text{m}$ pore size syringe filter the trend previously seen, disappears.

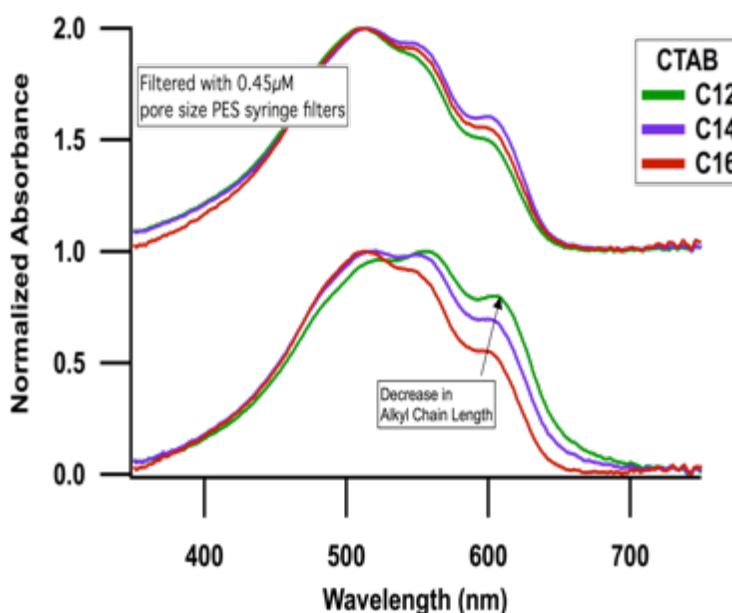


Figure 4.7: P3HT nanoparticles made with CTAB type surfactants varying the hydrocarbon chain length C12 (green), C14 (purple) and C16 (red).

These samples were made in triplicate and *one of three* was filtered. The non-filtered samples absorbance look almost identical for C12 and C14 but the aggregate portion of the absorbance is decreased after filtration. On the other

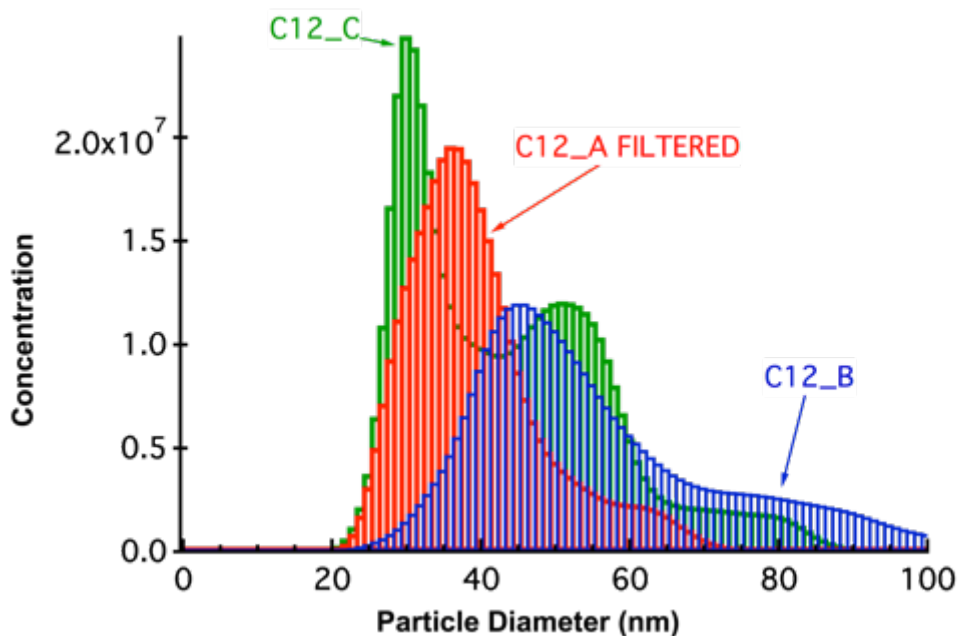


Figure 4.8: Particle size of nanoparticles made with CTAB type C12 chainlength surfactant

hand C16 appears to not be affected by filtration at all. C12 samples seem to be affected the greatest. If we look at the size distributions from nanosight, (Figure 4.8) there is no clear size expected for particles made with C12 surfactant.

However, one unfiltered sample has a bimodal distribution with a large concentration of small particles, where the other sample has the presence of much larger particles. The broad distributions and inconsistencies in size suggest possible particle aggregation, or increased coalescence while the oil phase is present. At the same time, filtering causes the lower energy portion (contributing to A_{0-0} and A_{0-1}) of the absorbance spectra to decrease. Therefore the filtrand, sample stuck in filter, is responsible for the change in UV signal and is of interest.

So, what could be happening during filtration? The filter and surfactant interact leaving NPs to aggregate and stick on the filter, or surfactant is buried in

the nanoparticle leaving some NPs without surface coverage. It is possible that the cationic surfactant dissolves in the oil phase during the emulsion and allows for much larger particles to form and clog the filter.

4.3.1 Solubility of Surfactant in Oil Phase

To see if CTAB was dissolving in the oil phase and interacting with P3HT or causing the polymer to aggregate we looked at solutions of P3HT and added in CTAB. There is a clear emergence of aggregates, much like what we saw in toluene (Chapter 3) and the peak at ~ 625 nm grows over time. Therefore, CTAB is in fact soluble in chloroform⁸ and can influence the aggregate structure. Future studies could investigate the way in which CTAB is causing P3HT to aggregate, and elucidate further ways to influence internal aggregate structure of P3HT NPs

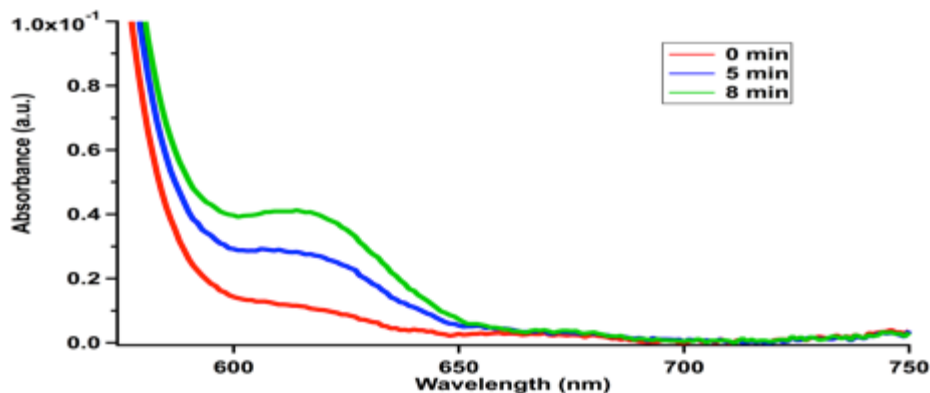


Figure 4.9: Absorbance Spectra of P3HT in CHCl_3 with the addition of CTAB over time, $t=0$ min (red), $t=5$ min (blue), $t=8$ min (green)

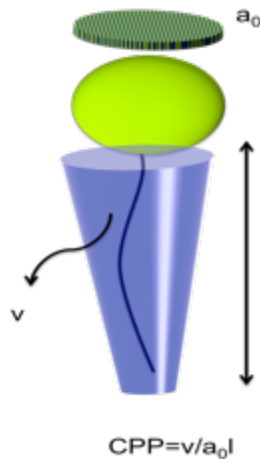


Figure 4.10: Critical packing parameter for amphiphiles, geometry defines what shape micelle to expect for self-assembly in water.

4.4 Nonionic Surfactants

Nonionic surfactants are of interest because of the shapes they self-assemble into. Surfactants generally follow a geometric constraint, the critical packing parameter (CPP), when self assembling in water (Figure 4.10). For SDS and CTAB the head groups are large and charged so they end up with a cone type geometry which leads to spherical micelles. Nonionic surfactants can become more like rods and pack into planar structures.⁹⁻¹¹

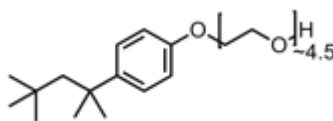


Figure 4.11: Molecular structure of nonionic surfactant, Triton X-45

4.41 Triton X-45

Beginning with a commercial nonionic surfactant, Triton X-45 (Pictured in figure 4.11) P3HT NPs were made while varying the surfactant concentration. In figure 4.12 the UV of unfiltered samples is shown, and towards the low end of triton concentration the A_{0-0} peak dominates the spectra. In this case, our peak ratio is over 1, meaning there is a majority of J-like aggregates contributing to the absorbance spectra.

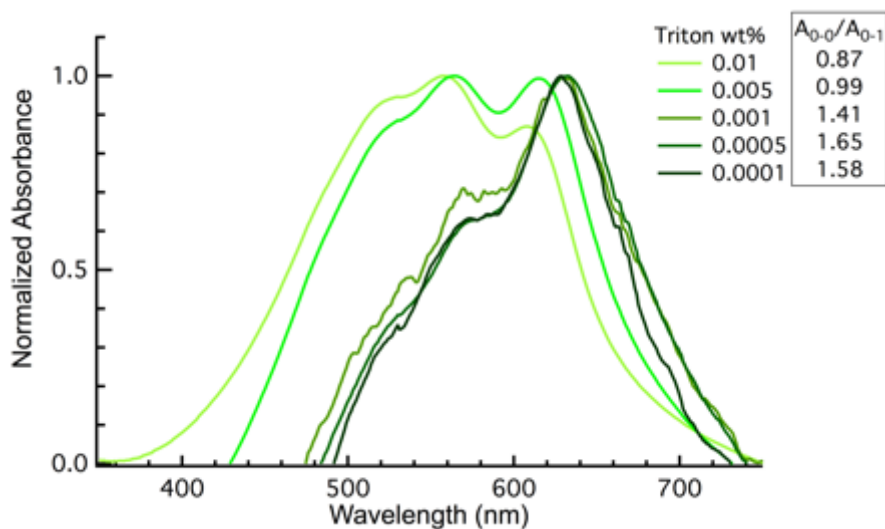


Figure 4.12 Absorbance spectra of P3HT NPs made with decreasing concentration of Triton X-45

Another interesting piece of data includes the potential shape change of P3HT nanoparticles made with Triton-X-45. From SEM the particle shape is shown to deviate from the typical sphere. Performing Energy Dispersive X-ray Spectroscopy (EDS) shows that the sample area scanned includes C, O, S, Si (wafer sample is deposited on), Na and Cl. Where a film of pure P3HT shows C, S, and B. The weight% ratio of C to S in pure P3HT films was found to be 5.5 and

around 7.8 in the particles made with Triton. The carbon ratio for the NPs versus the pure P3HT film is higher because of excess surfactant. In addition, samples of polystyrene nanoparticles (purely carbon) made with nonionic surfactants shows no sulfur present. However, the presence of Na and Cl makes the identification of P3HT ambiguous.

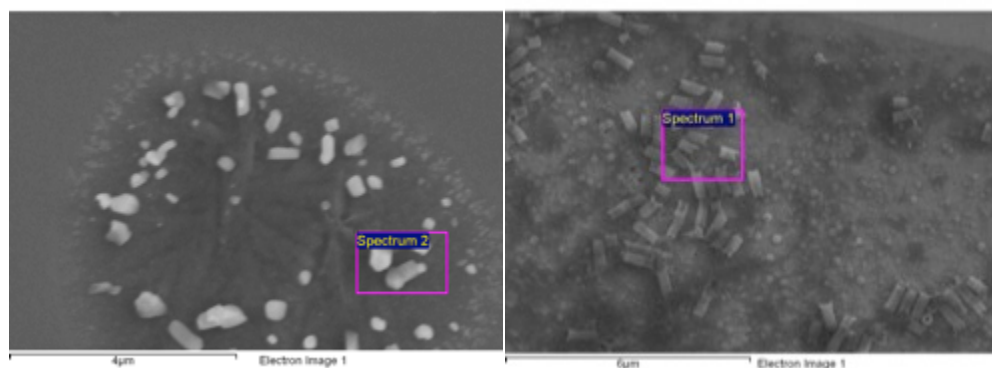


Figure 4.13: SEM images of nanoparticles made with nonionic surfactant. P3HT particles made with Triton X-45 (left) and polystyrene particles made with Tomadol 25-7 (right). The pink boxes are the areas EDAX was done on.

In some cases we observed purely salt crystals (Figure 4.14), however their size was much larger than observed particles and their behavior under the electron beam was different than the nanoparticles of irregular shapes. In support of the irregular shaped nanoparticles being P3HT, fluorescence microscopy (Figure 4.15) was used to look at a sample made from the same nanoparticle dispersion, to light up the P3HT. Although shape is out of the limit of resolution, we do see fluorescent particles of similar size to the irregular shaped nanoparticles seen in SEM.

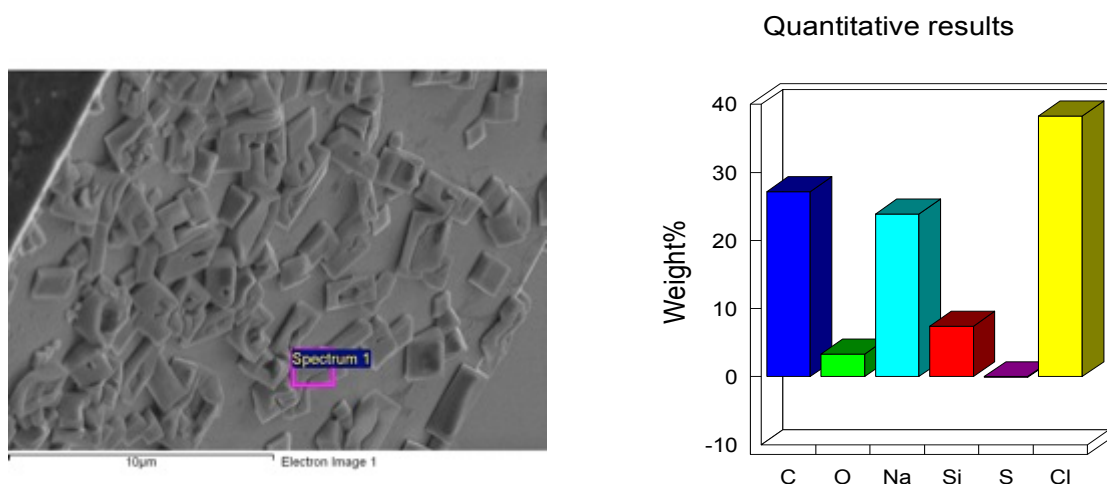


Figure 4.14: SEM image of possible NaCl crystals from dropcasting a dispersion of P3HT NPs, drying under air followed by a water rinse.

Unfortunately, the samples made are difficult to purify and fully characterize. The presumed particles can precipitate out of solution during evaporation or in general get stuck in a syringe filter. This discovery of cubic-like P3HT particles will be followed up with more in depth studies to discover the conditions that produce these interesting shapes and what electronic properties they exhibit. As for the stability of particles, we thought that the hydrophobic chain on Triton might not be long enough or very soluble in our emulsions.

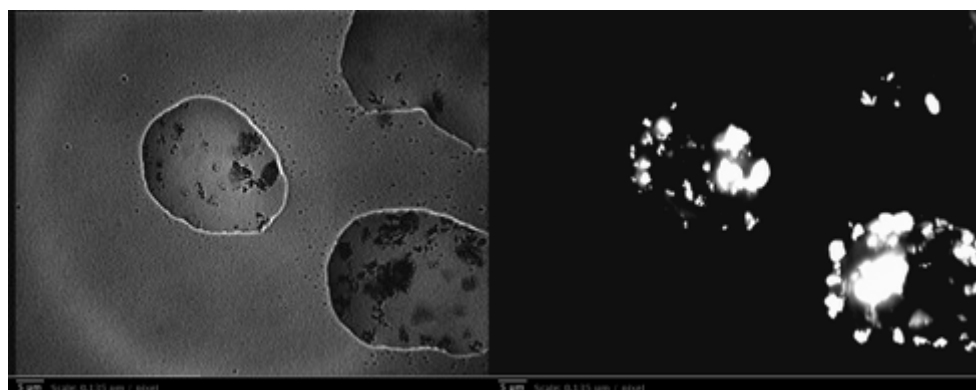


Figure 4.15: Confocal Fluorescence Microscopy images of P3HT particles made with Triton X-45 (left) light illumination (right) fluorescent image

4.4.2 CTAB-Triton Mixed Surfactant

Thinking about CTAB's ability to dissolve in the oil phase and Triton's apparent distaste for it, we decided to try a mixed surfactant system. The branched nature of Triton can potentially interact with CTAB's head group and together create a stable emulsion that can be tuned by varying the ratio of each.

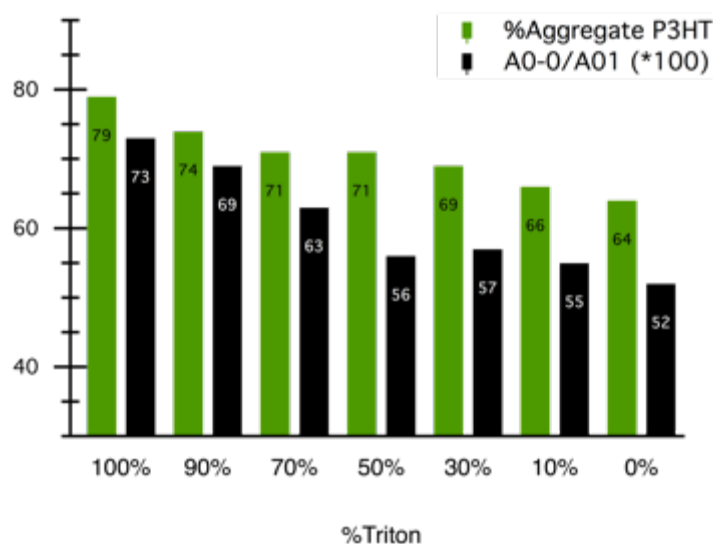


Figure 4.16: %Aggregate P3HT and A_{0-0}/A_{0-1} peak ratio from (x100) absorbance of P3HT NPs made with mixed surfactant of CTAB and Triton

There seems to be a trend with composition of CTAB to Triton and the peak ratio and percent aggregate. (Figure 4.16) When looking at a couple drop cast sample made from 70/30 and 50/50 with SEM, we actually see non-spherical particles and films with micron size pores at 70/30 ratio. The UV-Vis results show the potential of bi-surfactant systems to tune the internal structure of

a nanoparticle. While, the SEM images show the versatility in nanoscale to mesoscale assembly. This work needs to be explored further.

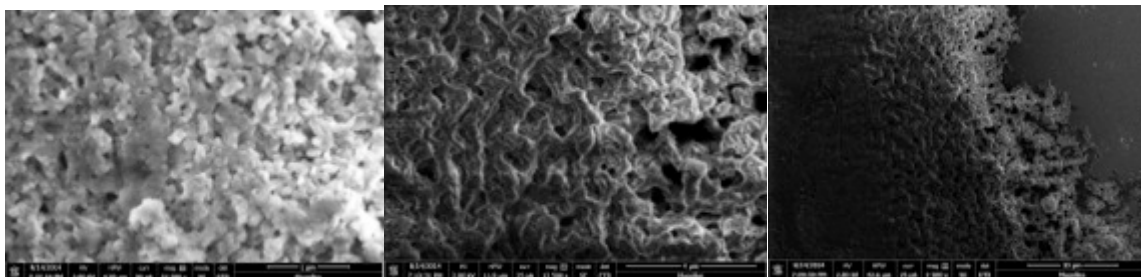


Figure 4.17: SEM of P3HT “NPs” made with varying ratios of CTAB to Triton 50/50(left), 70/30 (middle and right)

4.4.3 Tomadol

The last surfactant system we investigated was a linear nonionic surfactant, Tomadol (91-8) (Pictured in Figure 4.18). Similar to nonionic surfactant triton, we see intensity of the A_{0-0} absorbance peak rising and becoming the max (Table 4.2). And very similar to Triton we lose the interesting parts after filtering, so what is getting caught in the filter? SEM was used to look at the syringe filters membranes after filtering P3HT NP samples made with Tomadol. (Figure 4.19) The images show a large range of particle diameter and some deviation in shape. This work needs to be followed up

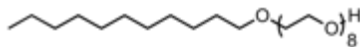


Figure 4.18: Molecular structure of Tomadol-91-8

Table 4.2 : Peak origin and ratio from UV-Vis, and size characterization of P3HT NPs made with Tomadol 91-8

	Before Filtration			After Filtration	
	1wt%	0.1wt%	0.01wt%	0.1wt%	0.01wt%
A_{0-0}	615	612	628	599	602
A_{0-0}/A_{0-1}	1.03	0.93	1.26	0.71	0.72
Diameter (nm)		184	188	123	130
SD		80	75	52	39

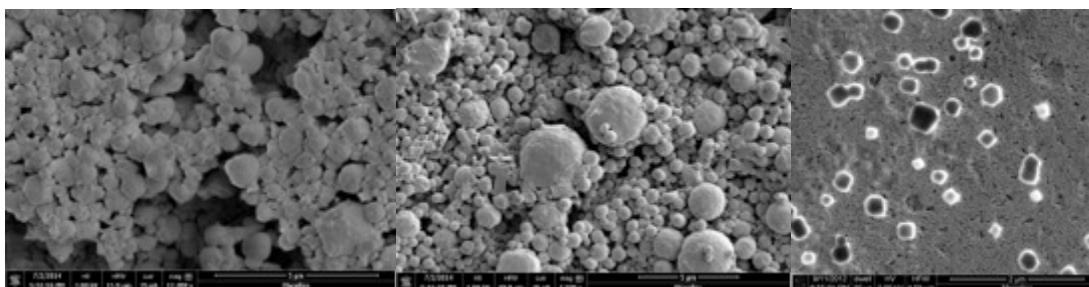


Figure 4.19: SEM of P3HT NPs clogging syringe filter membranes.

4.5 Conclusion

Through all our work on varying the surfactant used in the miniemulsion process to make nanoparticles we have shown a couple ways to tune the nanoparticles' internal structure and have ruled out others. Linear alkyl sodium sulfate surfactants seem to have no significant effect on the molecular packing of P3HT. However in the case of trimethylammonium bromide linear alkyl

surfactants we found a trend in aggregate structure with chainlength, decreasing the chain length increases the interchain ordering of P3HT. We can conclude that the surfactant must be soluble in the oil phase to have a significant impact.

As for nonionic surfactants, we see a large change in aggregate structure but the samples are highly disperse and not easily purified or characterized. Further investigation should be completed to better understand the mechanism of surfactant-polymer interactions in a miniemulsion.

4.6 References

- (1) Kwon, W. J.; Suh, D. H.; Chin, B. D.; Yu, J. Preparation of Polypyrrole Nanoparticles in Mixed Surfactants System. *J. Appl. Polym. Sci.* **2008**, *110*, 1324–1329.
- (2) Anilkumar, P.; Jayakannan, M. Single-Molecular-System-Based Selective Micellar Templates for Polyaniline Nanomaterials: Control of Shape, Size, Solid State Ordering, and Expanded Chain to Coillike Conformation. *Macromolecules* **2007**, *40*, 7311–7319.
- (3) Sui, J.; Zhang, L.; Travas-Sejdic, J.; Kilmartin, P. a. Synthesis of Poly(3,4-Ethylenedioxythiophene) Hollow Spheres in CTAB/DBS - Mixed Surfactant Solutions. *Macromol. Symp.* **2010**, *290*, 107–114.
- (4) Wang, Y.; Chen, W.; Zhou, D.; Xue, G. Synthesis of Conducting Polymer Spiral Nanostructures Using a Surfactant Crystallite Template. *Macromol. Chem. Phys.* **2009**, *210*, 936–941.
- (5) Antony, M. J.; Jayakannan, M. Molecular Template Approach for Evolution of Conducting Polymer Nanostructures: Tracing the Role of Morphology on Conductivity and Solid State Ordering. *J. Phys. Chem. B* **2010**, *114*, 1314–1324.
- (6) Fleischli, F. D.; Ghasdian, N.; Georgiou, T. K.; Stingelin, N. Tailoring the Optical Properties of poly(3-Hexylthiophene) by Emulsion Processing Using Polymeric Macrosurfactants. *J. Mater. Chem. C* **2015**, *3*, 2065–2071.
- (7) Xu, Z.; Yang, X.; Yang, Z. A Molecular Simulation Probing of Structure and Interaction for Supramolecular Sodium Dodecyl Sulfate/single-Wall Carbon Nanotube Assemblies. *Nano Lett.* **2010**, *10*, 985–991.
- (8) Sarrazin, P.; Chaussy, D.; Vurth, L.; Stephan, O.; Beneventi, D. Surfactant (TTAB) Role in the Preparation of 2,7-Poly(9,9-Dialkylfluorene-Co-Fluorenone) Nanoparticles by Miniemulsion. *Langmuir* **2009**, *25*, 6745–6752.
- (9) Rodríguez-Abreu, C.; García-Roman, M.; Kunieda, H. Rheology and Dynamics of Micellar Cubic Phases and Related Emulsions. *Langmuir* **2004**, *20*, 5235–5240.

- (10) Alam, M. M.; Sugiyama, Y.; Watanabe, K.; Aramaki, K. Phase Behavior and Rheology of Oil-Swollen Micellar Cubic Phase and Gel Emulsions in Nonionic Surfactant Systems. *J. Colloid Interface Sci.* **2010**, *341*, 267–272.
- (11) Paradies, H. H. Shape and Size of a Nonionic Surfactant Micelle. Triton X-100 in Aqueous Solution. *J. Phys. Chem.* **1980**, *84*, 599–607.

CHAPTER 5

FUTURE WORK

We have been interested in making nanoparticles of semiconducting polymers and small molecules primarily for the use in Organic Photovoltaics. The intermolecular packing of a semiconducting molecule influences the electronic properties of the overall material. We have presented a body of work that utilizes UV-Vis spectroscopy in order to characterize the internal structure of our P3HT nanoparticles. In previous work we have visually shown the structure within a cross-section of a P3HT nanoparticle utilizing High Resolution Transmission Electron Microscopy (HRTEM). The HRTEM micrograph (Figure 5.1) shows

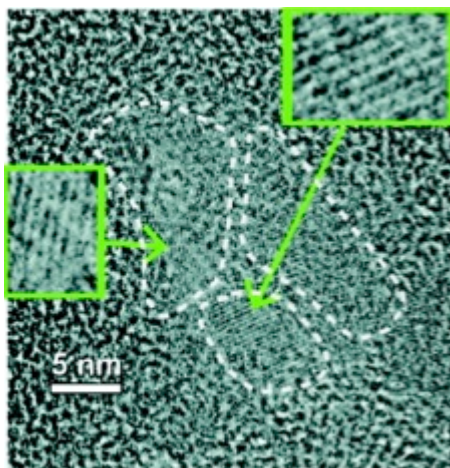


Figure 5.1 HRTEM image of a 116 nm particle. Crystalline domains of about 5–10 nm have been highlighted. The insets display the crystalline arrangements of each crystal. From these images, it is evident that the internal crystalline domains are randomly oriented.

crystalline domains of 5-10nm within a 116nm NP, that are randomly oriented. By utilizing electron tomography techniques we can reconstruct a three dimensional visualization of our nanoparticles.

The challenge comes with how to accurately capture the randomly oriented crystalline domains that may or may not be aligned properly with the sectioning of the particle. de With et. al. used cryo-HRTEM tomography to visualize P3HT nanowires in solution in three dimensions.¹ The vitrified solution is crucial to seeing the detailed pi-stacking because a typical nanowire dried on a TEM grid ends up with the lamellar stacks being perpendicular to the electron beam. The height versus width anisotropy of the wires is to blame for trapped orientation, however with a spherical nanoparticle we would be able to avoid that issue. With the correct TEM set-up we could investigate individual particles using a single-axis tilt series combined with gold nanoparticles as depth markers.² CryoET has been widely used in the life sciences as a strong investigative tool, however the field of organic nanostructures have yet to fully explore the 3D possibilities.

Visualizing P3HT NPs in three dimensions opens the door to correlating structural similarities among nanoparticles to their electronic properties. It can also enhance our understanding of particle formation, such as the actual amount and locations of aggregate or amorphous P3HT within the particle. Even more exciting as seen in chapter 4 with nonionic surfactants our particle shape becomes more anisotropic, giving the opportunity to study the effects of curvature

on a forming particle and P3HT aggregation. We can also have a deeper understanding of what size, orientation or location of a crystalline domain can be correlated to UV-Vis absorption characteristics. All of this comes back to the overarching goal of understanding structure function properties and the more we know the better technology we can create.

Building upon the research presented in this dissertation, visualizing the internal structure of the nanoparticle is the final puzzle piece to understand the effect of fabrication.

5.1 References

- (1) Wirix, M. J. M.; Bomans, P. H. H.; Friedrich, H.; Sommerdijk, N. A. J. M.; de With, G. Three-Dimensional Structure of P3HT Assemblies in Organic Solvents Revealed by Cryo-TEM. *Nano Lett.* **2014**, *14*, 2033–2038.
- (2) Nudelman, F.; de With, G.; Sommerdijk, N. a. J. M. Cryo-Electron Tomography: 3-Dimensional Imaging of Soft Matter. *Soft Matter* **2011**, *7*, 17.
- (3) Baghgar, M.; Labastide, J. A.; Bokel, F.; Hayward, R. C.; Barnes, M. D. Effect of Polymer Chain Folding on the Transition from H- to J-Aggregate Behavior in P3HT Nanofibers. *J. Phys. Chem. C* **2014**, *118*, 2229–2235.

APPENDIX
EXPERIMENTAL SECTION

CHAPTER 2 & 3

Materials

P3HT (4002-EE, $M_w = 52.3$ kDa, $\bar{D} = 2.15$ and regio-regularity = 90-93%) was purchased from commercial vendors. Sodium dodecyl sulfate (SDS), Cetlytrimethylammonium Bromide (CTAB), , were purchased from Sigma Aldrich. Solvents were purchased from Fisher (optima grade). Purified water (resistance 10 Mohms) was used for the synthesis of nanoparticles

Nanoparticle Fabrication

Synthesis of P3HT Nanoparticles. In a typical synthesis of P3HT nanoparticles, P3HT of a desired concentration was dissolved in a desired organic solvent. This solution was slightly warmed to ensure the complete solubility of P3HT. P3HT of 0.5 mg/mL concentration is bright orange in color for all three organic solvents used in this study. P3HT of 5 mg/mL concentration is bright orange color in chloroform and chloroform/toluene mixtures, whereas in toluene the solution is dark red. SDS solutions of desired concentration were prepared using purified water, then warmed and bath sonicated to ensure complete solubility. During the preparation of SDS solutions, caution was taken to prevent foaming by not shaking the solution vigorously to solubilize SDS. Also, during the synthesis of nanoparticles, the solution was transferred slowly via syringe. SDS solutions were filtered through syringe filters before use in the

synthesis of nanoparticles. A 2.5 mL aliquot of SDS solution was taken in a 20mL vial and ~0.35mL P3HT solution was taken in a 7 mL vial. Both solutions were sonicated in a MODEL 50T Aquasonic bath, for 10 s, and 0.25 mL of P3HT solution was immediately injected rapidly into the SDS solution using a 1 mL syringe fitted with a 22G 1/2 needle. The resulting solution was immediately ultrasonicated using a MISONIX SONICATOR 3000 with microprobe tip, for 2 min at 6 W power. During ultrasonication, the probe was submerged halfway into the solution at the same time not touching the vial throughout the ultrasonication. After ultrasonication, a magnetic stir bar was added into the emulsion and the vial was immersed into a preheated oil bath to evaporate organic solvent. The temperature of oil bath was maintained at ~85°C and the vial was immersed into the oil bath up to the emulsion level. The vial was heated for 15 min in the case of chloroform or toluene/chloroform mixture emulsions and was heated for ~50 min in the case of toluene emulsions. The nanoparticle suspension was allowed to come to room temperature and was filtered through a PES membrane with 0.22 µm pore size and 33mm in diameter to remove micrometer size impurities before

Instrumentation

Size and zeta potential were estimated using a Malvern Nanosize ZS dynamic light scattering instrument (CONTIN software). UV-Vis absorption spectra were measured with a Shimadzu UV 36000PC spectrometer in the

Polymer-Based Materials Harvesting Solar Energy (PHASE) EFRC (Energy Frontier Research Center at the University of Massachusetts Amherst) laboratory.

CHAPTER 4

Materials

P3HT (#RMI-001E Lot# BS23-02, Mw=36kDa, \bar{D} = 2.3, regioregularity ~96%) was purchased from commercial vendors. Sodium dodecyl sulfate (SDS), Cetlytrimethylammonium Bromide (CTAB), Sodium octadecyl sulfate(S18S), sodium tetradecyl sulfate, sodium octyl sulfate, Dodecyltrimethylammonium bromide, Myristyltrimethylammonium bromide, Triton X-45, were purchased from Sigma Aldrich. Tomadol 25-7 and Tomadol 91-8 were from J.H. Hess. Solvents were purchased from Fisher (optima grade). Purified water (resistance 10 Mohms) was used for the synthesis of nanoparticles

Nanoparticle Fabrication

In a typical synthesis of P3HT nanoparticles, P3HT of a desired concentration was dissolved in a desired organic solvent. This solution was slightly warmed to ensure the complete solubility of P3HT. The 5mg/mL P3HT solution in chloroform was bright orange in color. Surfactant solutions of desired concentration were prepared using purified water, then warmed and bath sonicated to ensure complete solubility. During the preparation of surfactant solutions, caution was taken to prevent foaming by not shaking the solution

vigorously. At high concentrations of S18S the solutions remained cloudy and were heated to ensure homogeneity and sonicated for 30 seconds immediately prior to taking aliquots. Both the P3HT solution and Surfactant solutions were kept in an aluminum block on a hot plate $\sim 30^{\circ}\text{C}$ while not in use to prevent aggregation. A 3 mL aliquot of surfactant solution was taken in a 15 mL polypropylene conical tube and $\sim 0.3\text{ mL}$ P3HT solution was immediately injected rapidly into the surfactant solution using a 1 mL syringe fitted with a 22G11/2 needle. The resulting solution was immediately ultrasonicated for 2 min at 20% max amplitude power. During ultrasonication, the probe was submerged to the point where the tube begins to taper. The tube was placed in an ice bath (tall enough to cover the emulsion). After ultrasonication, the emulsion was poured into a 20 mL glass vial and a magnetic stir bar was added into the emulsion. The vial was placed into a preheated fitted aluminum block to evaporate organic solvent. The vial was heated for 15 min for evaporation temperatures of 80°C . The nanoparticle suspension was allowed to come to room temperature and was filtered through a PES membrane with 0.22 μm , or 0.45 μm pore size and 33 mm diameter to remove micrometer size impurities before characterization

Instrumentation

Size was measured using a NS500 Nanosight, Nanoparticle Tracking Analysis instrument UV-Vis absorption spectra were measured with a Shimadzu UV-2401PC. SEM images and EDS information were obtained using a FEI

Magellan 400 Field Emission scanning electron microscope with a Oxford 80mm²
X-Max Energy Dispersive X-Ray Spectrometer.

BIBLIOGRAPHY

- Alam, M. M.; Sugiyama, Y.; Watanabe, K.; Aramaki, K. Phase Behavior and Rheology of Oil-Swollen Micellar Cubic Phase and Gel Emulsions in Nonionic Surfactant Systems. *J. Colloid Interface Sci.* **2010**, *341*, 267–272.
- Almería, B.; Gomez, A. Electro spray synthesis of monodisperse polymer particles in a broad (60nm-2 μ m) diameter range: Guiding principles and formulation recipes. *J. Colloid Interface Sci.* **2014**, *417*, 121–130.
- Anilkumar, P.; Jayakannan, M. Single-Molecular-System-Based Selective Micellar Templates for Polyaniline Nanomaterials: Control of Shape, Size, Solid State Ordering, and Expanded Chain to Coillike Conformation. *Macromolecules* **2007**, *40*, 7311–7319.
- Antony, M. J.; Jayakannan, M. Molecular Template Approach for Evolution of Conducting Polymer Nanostructures: Tracing the Role of Morphology on Conductivity and Solid State Ordering. *J. Phys. Chem. B* **2010**, *114*, 1314–1324.
- Bag, M.; Gehan, T. S.; Algaier, D. D.; Liu, F.; Nagarjuna, G.; Lahti, P. M.; Russell, T. P.; Venkataraman, D. Efficient charge transport in assemblies of surfactant-stabilized semiconducting nanoparticles. *Adv. Mater.* **2013**, *25*, 6411–6415.
- Baghgar, M.; Labastide, J. A.; Bokel, F.; Hayward, R. C.; Barnes, M. D. Effect of Polymer Chain Folding on the Transition from H- to J-Aggregate Behavior in P3HT Nanofibers. *J. Phys. Chem. C* **2014**, *118*, 2229–2235.
- Bartlett, P.; Ottewill, R. H.; Pusey, P. N. Superlattice formation in binary mixtures of hard-sphere colloids. *Phys. Rev. Lett.* **1992**, *68*, 3801–3804.
- Beaujuge, P. M.; Fréchet, J. M. J. Molecular design and ordering effects in π -functional materials for transistor and solar cell applications. *J. Am. Chem. Soc.* **2011**, *133*, 20009–20029.
- Benanti, T. L.; Venkataraman, D. Organic solar cells: an overview focusing on active layer morphology. *Photosynth. Res.* **2006**, *87*, 73–81.
- Bishop, K. J. M.; Wilmer, C. E.; Soh, S.; Grzybowski, B. A. Nanoscale forces and their uses in self-assembly. *Small* **2009**, *5*, 1600–1630.
- Chen, Y. C.; Dimonie, V.; El-Aasser, M. S. Role of surfactant in composite latex particle morphology. *J. Appl. Polym. Sci.* **1992**, *45*, 487–499.
- Chen, J.-T.; Hsu, C.-S. Conjugated polymer nanostructures for organic solar cell applications. *Polym. Chem.* **2011**, *2*, 2707.

- Chen, P.-Y.; Rassamesard, A.; Chen, H.-L.; Chen, S.-A. Conformation and Fluorescence Property of Poly(3-hexylthiophene) Isolated Chains Studied by Single Molecule Spectroscopy: Effects of Solvent Quality and Regioregularity. *Macromolecules* **2013**.
- Chen, Y.; Zhao, Y.; Liang, Z. Solution processed organic thermoelectrics: towards flexible thermoelectric modules. *Energy Environ. Sci.* **2015**, *8*, 401–422.
- Chu, H.-H.; Hseih, R.-T. Effect of Surfactant Configurations on Miniemulsion Polymerization. *J. Macromol. Sci. Part A* **1995**, *32*, 1353–1363.
- Clark, J.; Chang, J. F.; Spano, F. C.; Friend, R. H.; Silva, C. Determining exciton bandwidth and film microstructure in polythiophene films using linear absorption spectroscopy. *Appl. Phys. Lett.* **2009**, *94*, 163306–1 – 3.
- Collier, C. P.; Vossmeier, T.; Heath, J. R. Nanocrystal superlattices. *Annu. Rev. Phys. Chem.* **1998**, *49*, 371–404.
- Dang, M. T.; Hirsch, L.; Wantz, G. P3HT:PCBM, Best Seller in Polymer Photovoltaic Research. *Adv. Mater.* **2011**, *23*, 3597–3602.
- Dang, M. T.; Hirsch, L.; Wantz, G.; Wuest, J. D. Controlling the Morphology and Performance of Bulk Heterojunctions in Solar Cells. Lessons Learned from the Benchmark Poly(3-hexylthiophene):[6,6]-Phenyl-C 61 -butyric Acid Methyl Ester System. *Chem. Rev.* **2013**, *113*, 3734–3765.
- Darwis, D.; Holmes, N.; Elkington, D.; David Kilcoyne, A. L.; Bryant, G.; Zhou, X.; Dastoor, P.; Belcher, W. Surfactant-free nanoparticulate organic photovoltaics. *Sol. Energy Mater. Sol. Cells* **2014**, *121*, 99–107.
- Dennler, G.; Scharber, M. C.; Brabec, C. J. Polymer-fullerene bulk-heterojunction solar cells. *Advanced Materials*, 2009, *21*, 1323–1338.
- Derjaguin, B. On the repulsive forces between charged colloid particles and on the theory of slow coagulation and stability of lyophobic sols. *Transactions of the Faraday Society*, 1940, *35*, 203.
- Evans, R. C. Harnessing self-assembly strategies for the rational design of conjugated polymer based materials. *J. Mater. Chem. C* **2013**, *1*, 4190.
- Fleischli, F. D.; Ghasdian, N.; Georgiou, T. K.; Stingelin, N. Tailoring the Optical Properties of poly(3-Hexylthiophene) by Emulsion Processing Using Polymeric Macrosurfactants. *J. Mater. Chem. C* **2015**, *3*, 2065–2071
- Gehan, T. S.; Bag, M.; Renna, L. A.; Shen, X.; Algaier, D. D.; Lahti, P. M.; Russell, T. P.; Venkataraman, D. Multiscale Active Layer Morphologies for Organic Photovoltaics Through Self-Assembly of Nanospheres. *Nano Lett.* **2014**, *14*, 5238–5243.

- He, Z.; Wu, H.; Cao, Y. Recent advances in polymer solar cells: realization of high device performance by incorporating water/alcohol-soluble conjugated polymers as electrode buffer layer. *Adv. Mater.* **2014**, *26*, 1006–1024.
- Hong, Y.; Lam, J. W. Y.; Tang, B. Z. Aggregation-induced emission: phenomenon, mechanism and applications. *Chem. Commun.* **2009**, 4332.
- Horn, D.; Rieger, J. Organic Nanoparticles in the Aqueous Phase-Theory, Experiment, and Use. *Angew. Chemie Int. Ed.* **2001**, *40*, 4330–4361.
- Hu, S.; Dyck, O.; Chen, H.; Hsiao, Y.; Hu, B.; Duscher, G.; Dadmun, M.; Khomami, B. The impact of selective solvents on the evolution of structure and function in solvent annealed organic photovoltaics. *RSC Adv.* **2014**, *4*, 27931.
- Huang, Y.; Kramer, E. J.; Heeger, A. J.; Bazan, G. C. Bulk heterojunction solar cells: morphology and performance relationships. *Chem. Rev.* **2014**, *114*, 7006–7043.
- Ikkala, O.; ten Brinke, G. Functional materials based on self-assembly of polymeric supramolecules. *Science* **2002**, *295*, 2407–2409.
- Jackson, N. E.; Savoie, B. M.; Marks, T. J.; Chen, L. X.; Ratner, M. A. The Next Breakthrough for Organic Photovoltaics? *J. Phys. Chem. Lett.* **2015**, *6*, 77–84.
- Jochum, F. D.; Theato, P. Temperature- and light-responsive smart polymer materials. *Chem. Soc. Rev.* **2013**, *42*, 7468–7483.
- Johnson, C. E.; Boucher, D. S. Poly(3-hexylthiophene) aggregate formation in binary solvent mixtures: An excitonic coupling analysis. *J. Polym. Sci. Part B Polym. Phys.* **2014**, *52*, 526–538.
- Jou, J.-H.; Kumar, S.; Agrawal, A.; Li, T.-H.; Sahoo, S. Approaches for fabricating high efficiency organic light emitting diodes. *J. Mater. Chem. C* **2015**, *3*, 2974–3002.
- Khim, D.; Baeg, K.-J.; Caironi, M.; Liu, C.; Xu, Y.; Kim, D.-Y.; Noh, Y.-Y. Control of Ambipolar and Unipolar Transport in Organic Transistors by Selective Inkjet-Printed Chemical Doping for High Performance Complementary Circuits. *Adv. Funct. Mater.* **2014**, *24*, 6252–6261.
- Kietzke, T.; Neher, D.; Landfester, K.; Montenegro, R.; Güntner, R.; Scherf, U. Novel approaches to polymer blends based on polymer nanoparticles. *Nat. Mater.* **2003**, *2*, 408–412.
- Kim, J.; Swager, T. Control of conformational and interpolymer effects in conjugated polymers. *Nature* **2001**, *411*, 1030–1034.

- Koch, F. P. V.; Rivnay, J.; Foster, S.; Müller, C.; Downing, J. M.; Buchaca-Domingo, E.; Westacott, P.; Yu, L.; Yuan, M.; Baklar, M.; et al. The impact of molecular weight on microstructure and charge transport in semicrystalline polymer semiconductors—poly(3-hexylthiophene), a model study. *Prog. Polym. Sci.* **2013**, *38*, 1978–1989.
- Kumar, P.; Mehta, A.; Mahurin, S. M.; Dai, S.; Dadmun, M. D.; Sumpter, B. G.; Barnes, M. D. Formation of oriented nanostructures from single molecules of conjugated polymers in microdroplets of solution: The role of solvent. *Macromolecules* **2004**, *37*, 6132–6140.
- Kwon, W. J.; Suh, D. H.; Chin, B. D.; Yu, J. Preparation of Polypyrrole Nanoparticles in Mixed Surfactants System. *J. Appl. Polym. Sci.* **2008**, *110*, 1324–1329.
- Labastide, J. A.; Baghgar, M.; Dujovne, I.; Venkatraman, B. H.; Ramsdell, D. C.; Venkataraman, D.; Barnes, M. D. Time- and Polarization-Resolved Photoluminescence of Individual Semicrystalline Polythiophene (P3HT) Nanoparticles. *J. Phys. Chem. Lett.* **2011**, *2*, 2089–2093.
- Labastide, J. A.; Baghgar, M.; Dujovne, I.; Yang, Y.; Dinsmore, A. D.; Sumpter, B. G.; Venkataraman, D.; Barnes, M. D. Polymer nanoparticle superlattices for organic photovoltaic applications. *J. Phys. Chem. Lett.* **2011**, *2*, 3085–3091.
- Labastide, J. A.; Baghgar, M.; McKenna, A.; Barnes, M. D. Time- and Polarization-Resolved Photoluminescence Decay from Isolated Polythiophene (P3HT) Nanofibers. *J. Phys. Chem. C* **2012**, *116*, 23803–23811.
- Landfester, K. Miniemulsions for Nanoparticle Synthesis. *Anion Sens.* **2003**, 75–123.
- Landfester, K. Miniemulsion polymerization and the structure of polymer and hybrid nanoparticles. *Angew. Chemie Int. Ed.* **2009**, *48*, 4488–4507.
- Lecover, R.; Williams, N.; Markovic, N.; Reich, D. H.; Naiman, D. Q.; Katz, H. E. Next-generation polymer solar cell materials: Designed control of interfacial variables. *ACS Nano* **2012**, *6*, 2865–2870.
- Lee, J.; Balakrishnan, S.; Cho, J.; Jeon, S.; Kim, J. Detection of adulterated gasoline using colorimetric organic microfibers. *J. Mater. Chem.* **2011**, *21*, 2648.
- Machui, F.; Langner, S.; Zhu, X.; Abbott, S.; Brabec, C. J. Determination of the P3HT:PCBM solubility parameters via a binary solvent gradient method: Impact of solubility on the photovoltaic performance. *Sol. Energy Mater. Sol. Cells* **2012**, *100*, 138–146.

- Maskey, S.; Osti, N. C.; Perahia, D.; Grest, G. S. Internal correlations and stability of polydots, soft conjugated polymeric nanoparticles. *ACS Macro Lett.* **2013**, *2*, 700–704.
- Mason, T. G.; Wilking, J. N.; Meleson, K.; Chang, C. B.; Graves, S. M. Nanoemulsions: formation, structure, and physical properties. *J. Phys. Condens. Matter* **2006**, *18*, R635–R666.
- Mecerreyes, D. Polymeric ionic liquids: Broadening the properties and applications of polyelectrolytes. *Prog. Polym. Sci.* **2011**, *36*, 1629–1648.
- Millstone, J. E.; Kavulak, D. F. J.; Woo, C. H.; Holcombe, T. W.; Westling, E. J.; Briseno, A. L.; Toney, M. F.; Fréchet, J. M. J. Synthesis, Properties, and Electronic Applications of Size-Controlled Poly(3-hexylthiophene) Nanoparticles. *Langmuir* **2010**, *26*, 13056–13061.
- Moulé, a. J.; Meerholz, K. Controlling Morphology in Polymer–Fullerene Mixtures. *Adv. Mater.* **2008**, *20*, 240–245.
- Nagarjuna, G.; Baghgar, M.; Labastide, J. A.; Algaier, D. D.; Barnes, M. D.; Venkataraman, D. Tuning aggregation of poly(3-hexylthiophene) within nanoparticles. *ACS Nano* **2012**, *6*, 10750–10758.
- Nagarjuna, G.; Venkataraman, D. Strategies for controlling the active layer morphologies in OPVs. *J. Polym. Sci. Part B Polym. Phys.* **2012**, *50*, 1045–1056.
- Noriega, R.; Rivnay, J.; Vandewal, K.; Koch, F. P. V; Stingelin, N.; Smith, P.; Toney, M. F.; Salleo, A. A general relationship between disorder, aggregation and charge transport in conjugated polymers. *Nat. Mater.* **2013**, *12*, 1038–1044.
- Nudelman, F.; de With, G.; Sommerdijk, N. a. J. M. Cryo-Electron Tomography: 3-Dimensional Imaging of Soft Matter. *Soft Matter* **2011**, *7*, 17.
- Panzer, F.; Bäessler, H.; Lohwasser, R.; Thelakkat, M.; Köhler, A. The Impact of Polydispersity and Molecular Weight on the Order–Disorder Transition in Poly(3-hexylthiophene). *J. Phys. Chem. Lett.* **2014**, *5*, 2742–2747.
- Paquin, F.; Yamagata, H.; Hestand, N. J.; Sakowicz, M.; Bérubé, N.; Côté, M.; Reynolds, L. X.; Haque, S. A.; Stingelin, N.; Spano, F. C.; et al. Two-dimensional spatial coherence of excitons in semicrystalline polymeric semiconductors: Effect of molecular weight. *Phys. Rev. B - Condens. Matter Mater. Phys.* **2013**, *88*, 155202.
- Paradies, H. H. Shape and Size of a Nonionic Surfactant Micelle. Triton X-100 in Aqueous Solution. *J. Phys. Chem.* **1980**, *84*, 599–607.
- Patterson, J. P.; Robin, M. P.; Chassenieux, C.; Colombani, O.; O'Reilly, R. K. The analysis of solution self-assembled polymeric nanomaterials. *Chem. Soc. Rev.* **2014**, *43*, 2412–2425.

- Pauling, L. The Principles Determining the Structure of Complex Ionic Crystals. *J. Am. Chem. Soc.* **1929**, *51*, 1010–1026.
- Potai, R.; Traiphol, R. Controlling chain organization and photophysical properties of conjugated polymer nanoparticles prepared by reprecipitation method: The effect of initial solvent. *J. Colloid Interface Sci.* **2013**, *403*, 58–66.
- Reineke, S.; Lindner, F.; Schwartz, G.; Seidler, N.; Walzer, K.; Lüssem, B.; Leo, K. White organic light-emitting diodes with fluorescent tube efficiency. *Nature* **2009**, *459*, 234–238.
- Rodríguez-Abreu, C.; García-Roman, M.; Kunieda, H. Rheology and Dynamics of Micellar Cubic Phases and Related Emulsions. *Langmuir* **2004**, *20*, 5235–5240.
- Sanders, J.; Murray, M. Ordered arrangements of spheres of two different sizes in opal. *Nature* **1978**, *275*, 201–202.
- Sarrazin, P.; Chaussy, D.; Vurth, L.; Stephan, O.; Beneventi, D. Surfactant (TTAB) Role in the Preparation of 2,7-Poly(9,9-Dialkylfluorene-Co-Fluorenone) Nanoparticles by Miniemulsion. *Langmuir* **2009**, *25*, 6745–6752.
- Schacher, F. H.; Rugar, P. A.; Manners, I. Functional block copolymers: nanostructured materials with emerging applications. *Angew. Chemie Int. Ed.* **2012**, *51*, 7898–7921.
- Scharsich, C.; Lohwasser, R. H.; Sommer, M.; Asawapirom, U.; Scherf, U.; Thelakkat, M.; Neher, D.; Köhler, A. Control of aggregate formation in poly(3-hexylthiophene) by solvent, molecular weight, and synthetic method. *J. Polym. Sci. Part B Polym. Phys.* **2012**, *50*, 442–453.
- Schreiber, E.; Ziener, U.; Manzke, A.; Plettl, A.; Ziemann, P.; Landfester, K. Preparation of Narrowly Size Distributed Metal-Containing Polymer Latexes by Miniemulsion and Other Emulsion Techniques: Applications for Nanolithography. *Chem. Mater.* **2009**, *21*, 1750–1760.
- Servaites, J. D.; Ratner, M. A.; Marks, T. J. Organic solar cells: A new look at traditional models. *Energy Environ. Sci.* **2011**, *4*, 4410.
- Søndergaard, R. R.; Hösel, M.; Krebs, F. C. Roll-to-Roll fabrication of large area functional organic materials. *J. Polym. Sci. Part B Polym. Phys.* **2013**, *51*, 16–34.
- Spano, F. C. Modeling disorder in polymer aggregates: The optical spectroscopy of regioregular poly(3-hexylthiophene) thin films. *J. Chem. Phys.* **2005**, *122*, 234701.

- Spano, F. C. Absorption in regio-regular poly(3-hexyl)thiophene thin films: Fermi resonances, interband coupling and disorder. *Chem. Phys.* **2006**, *325*, 22–35.
- Spano, F. C. Excitons in conjugated oligomer aggregates, films, and crystals. *Annu. Rev. Phys. Chem.* **2006**, *57*, 217–243.
- Spano, F. C. The spectral signatures of frenkel polarons in H- And J-aggregates. *Acc. Chem. Res.* **2010**, *43*, 429–439.
- Stupp, S. I.; Palmer, L. C. Supramolecular Chemistry and Self-Assembly in Organic Materials Design. *Chem. Mater.* **2014**, *26*, 507–518.
- Sui, J.; Zhang, L.; Travas-Sejdic, J.; Kilmartin, P. a. Synthesis of Poly(3,4-Ethylenedioxythiophene) Hollow Spheres in CTAB/DBS - Mixed Surfactant Solutions. *Macromol. Symp.* **2010**, *290*, 107–114.
- Verwey, E. J. W. Theory of the stability of lyophobic colloids. *J. Phys. Colloid Chem.* **1947**, *51*, 631–636.
- Wang, Y.; Chen, W.; Zhou, D.; Xue, G. Synthesis of Conducting Polymer Spiral Nanostructures Using a Surfactant Crystallite Template. *Macromol. Chem. Phys.* **2009**, *210*, 936–941.
- Wang, T.; Dunbar, A. D. F.; Staniec, P. A.; Pearson, A. J.; Hopkinson, P. E.; MacDonald, J. E.; Lilliu, S.; Pizzey, C.; Terrill, N. J.; Donald, A. M.; et al. The development of nanoscale morphology in polymer:fullerene photovoltaic blends during solvent casting. *Soft Matter* **2010**, *6*, 4128.
- Wang, J.-T.; Wang, J.; Han, J.-J. Fabrication of advanced particles and particle-based materials assisted by droplet-based microfluidics. *Small* **2011**, *7*, 1728–1754.
- Wirix, M. J. M.; Bomans, P. H. H.; Friedrich, H.; Sommerdijk, N. A. J. M.; de With, G. Three-Dimensional Structure of P3HT Assemblies in Organic Solvents Revealed by Cryo-TEM. *Nano Lett.* **2014**, *14*, 2033–2038.
- Wong, T.-S.; Chen, T.-H.; Shen, X.; Ho, C.-M. Nanochromatography Driven by the Coffee Ring Effect. *Anal. Chem.* **2011**, 11–13.
- Woo, C. H.; Thompson, B. C.; Kim, B. J.; Toney, M. F.; Fréchet, J. M. J. The influence of poly(3-hexylthiophene) regioregularity on fullerene-composite solar cell performance. *J. Am. Chem. Soc.* **2008**, *130*, 16324–16329.
- Xu, Z.; Yang, X.; Yang, Z. A Molecular Simulation Probing of Structure and Interaction for Supramolecular Sodium Dodecyl Sulfate/single-Wall Carbon Nanotube Assemblies. *Nano Lett.* **2010**, *10*, 985–991.
- Xue, L.; Gao, X.; Zhao, K.; Liu, J.; Yu, X.; Han, Y. The formation of different structures of poly(3-hexylthiophene) film on a patterned substrate by dip coating from aged solution. *Nanotechnology* **2010**, *21*, 145303.

- Yassar, A.; Miozzo, L.; Gironda, R.; Horowitz, G. Rod–coil and all-conjugated block copolymers for photovoltaic applications. *Prog. Polym. Sci.* **2013**, *38*, 791–844.
- Yin, W.; Dadmun, M. A New Model for the Morphology of P3HT/PCBM Organic Photovoltaics from Small-Angle Neutron Scattering: Rivers and Streams. *ACS Nano* **2011**, *5*, 4756–4768.
- Zanetti-Ramos, B. G.; Fritzen-Garcia, M. B.; de Oliveira, C. S.; Pasa, A. A.; Soldi, V.; Borsali, R.; Creczynski-Pasa, T. B. Dynamic light scattering and atomic force microscopy techniques for size determination of polyurethane nanoparticles. *Mater. Sci. Eng. C* **2009**, *29*, 638–640.
- Zhao, K.; Xue, L.; Liu, J.; Gao, X.; Wu, S.; Han, Y.; Geng, Y. A New Method to Improve Poly(3-hexyl thiophene) (P3HT) Crystalline Behavior: Decreasing Chains Entanglement to Promote Order-Disorder Transformation in Solution. *Langmuir* **2010**, *26*, 471–477.
- Zhokhavets, U.; Erb, T.; Gobsch, G.; Al-Ibrahim, M.; Ambacher, O. Relation between absorption and crystallinity of poly(3-hexylthiophene)/fullerene films for plastic solar cells. *Chem. Phys. Lett.* **2006**, *418*, 347–350.